8-2020

A Comparison Between Ultrasonic Guided Wave Leakage and Half-Cell Potential Methods in Detection of Corrosion in Reinforced Concrete Structures

Ahmad Shoaib Amiri
University of Nebraska - Lincoln, shoaib7amiri@gmail.com

A COMPARISON BETWEEN ULTRASONIC GUIDED WAVE LEAKAGE AND HALF-CELL POTENTIAL METHODS IN DETECTION OF CORROSION IN REINFORCED CONCRETE DECKS

by

Ahmad Shoaib Amiri

A THESIS

Presented to the Faculty of

The Graduate College at the University of Nebraska

In Partial Fulfillment of Requirements

For the Degree of Master of Science

Major: Architectural Engineering

Under the Supervision of Professor Ece Erdogmus

Lincoln, Nebraska

August, 2020

A COMPARISON BETWEEN ULTRASONIC GUIDED WAVE LEAKAGE AND HALF-CELL POTENTIAL METHODS IN DETECTION OF CORROSION IN REINFORCED CONCRETE STRUCTURES

AHMAD SHOAIB AMIRI, M.S.

University of Nebraska, 2020

Advisor: Ece Erdogmus

Corrosion of reinforcing steel bars (rebar) in reinforced concrete decks can lead to serious structural issues in bridges. Ultrasonic Testing (UT) methods provide small wavelengths that can be used for early detection of several types of deterioration. The recently-developed Ultrasonic Guided Wave Leakage (UGWL) Method utilizes steel as the waveguide and measures the energy leaked into the surrounding concrete. Previous studies completed at University of Nebraska-Lincoln demonstrated that the measurements of the leaked energy using receivers from the concrete surface can successfully identify early stages of various flaws such as corrosion, delamination, and cracking. In this method, the longitudinal waves are generated along the rebar by a transmitter placed directly on the rebar, and recorded by an array of receivers on the concrete surface. Previous studies have shown promise in testing stretches of concrete decks as long as 10 feet using a single transmitter and an array of sensors placed 6 inches apart.

The primary goal of this Master's thesis is to demonstrate that the recently developed UGWL method has several advantages over the commonly used Half-Cell Potential (HCP) method in the detection of corrosion in reinforced concrete (RC) bridge decks. To achieve this goal, laboratory experiments as well as a pros-and-cons analysis is conducted. Laboratory specimens are placed in a corrosive environment by submerging them in 10% NaCl solution. These slabs were then monitored for 6 months. During this period, UGWL and half-cell potential

data were collected every 6 days. After testing was completed, chloride threshold levels (CTLs) were measured on cores taken from the specimens. The secondary goal of this thesis is to develop a quantitative correlation between UGWL data and CTLs, similar to those established between HCP and CTLs in the literature.

The experimental results demonstrated that the UGWL technique detected the corrosion activity approximately 21 days sooner than the HCP method. The findings also suggest that chloride content determined after the completion of the corrosion process, which lasted for 6 months, exceeded the standard chloride threshold levels; confirming that the selected method of inducing corrosion in the lab was successful.

DEDICATION

This thesis is dedicated to my parents, wife, and brothers whose love, support and sacrifice made it possible for me to pursue my dreams.

ACKNOWLEDGEMENT

I would like to express my sincere gratitude and appreciation to my advisor, Dr. Ece Erdogmus for her consistent support, guidance, and encouragement. My achievements would not have been possible without her help. I would also like to thank Dr. George Morcous, Dr. Chungwook Sim, Dr. Eric Garcia for their willingness to serve on my committee and provide their assistance.

I wish to express my sincere appreciation to Mr. Michael Schuller and everyone at Atkinson-Noland and Associates for their valued support, insight, and providing some of the equipment needed to carry out the experiments in this dissertation.

The Nebraska Department of Transportation (NDOT) is acknowledged for the financial support and opportunities they provided, especially Mrs. Fouad Jaber, Babrak Niazi, Mike Vigil, and Ms. Lieska Halsey.

I would like to acknowledge the undergraduate students, especially Mitchael Sieh, Uziel Ramos, Dylan Thompson, and Ben Schnatz who contributed in this research and assisted in data collection. The Durham Science Center at the University of Nebraska-Omaha is acknowledged for their support with chloride testing on concrete samples. I would also like to thank the laboratory technicians at the University of Nebraska-Lincoln who provided assistance with the experimental work in this research.

Without my family, and specially the love of my life, Zhila Amiry, this accomplishment would not have been possible. Special thanks to my amazing parents whose love, kindness, and

sacrifices have always been with me. Thanks to my brothers for motivating me in every step of this journey.

TABLE OF CONTENT

LIST OF FIGURES

LIST OF TABLES

CHAPTER 1

INTRODUCTION

1.1. Motivation and Background

Reinforced concrete (RC) is the most commonly used construction material in the United States and abroad. For instance, RC makes up more than half of the bridges in the U.S. (Hartt et al., 2004). However, the integrity of RC structures is often affected by the detrimental effects of environmental factors, leading to flaws such corrosion and delamination. RC bridge decks are especially highly prone to these flaws. Two primary factors for the onset of corrosion are concrete carbonation and chlorides. The corrosion behavior of the steel in concrete is arguably a primary durability and serviceability concern worldwide. Three major causes of bridge decks deteriorations are chloride-induced corrosion, freeze-thaw cycles, and poor construction practices (Hema & Guthrie, 2004). It has been stated that the annual repair costs related to corrosion problems in highway bridges is around $8.3 billion, including $2 billion only for bridge decks (Cui, 2012). Thus, it is necessary to detect the corrosion before it becomes a serious problem.

With the increased awareness of the significance of damage detection technologies, researchers have used numerous structural health monitoring (SHM) systems for the early detection of these flaws in RC. Non-destructive testing (NDT) techniques have been employed for the inspection of bridge decks without long-term traffic obstructions. NDT evaluations may include several techniques such as acoustic, electrochemical, electromagnetic and visual inspection (Scott et al., 2003).

Current NDT methods can detect flaws that develop beyond a certain size, but they are not effective in identifying the onset of deteriorations in the bridge decks. Among different NDT techniques, the Ultrasonic Testing (UT) has the most potential for identification of the smallest cracks and voids of different types successfully. Since UT is sensitive to defects present in the test materials, this method can be used to detect very small changes in the amount of leaked energy. Garcia et al. (2019) proposed an ultrasonic guided wave leakage (UGWL) method that is capable of detecting delaminations as small as 0.2 mm (0.008 in.). This study aims to demonstrate the potential of the recently-developed UGWL method in identifying the onset and progression of corrosion in reinforced concrete structures, and to identify its advantages over the traditional Half-cell potential method.

1.2. Research Goals and Objectives

The primary goal of this Master's thesis is to demonstrate that the newly-developed ultrasonic testing method, i.e. the UGWL method has several advantages over the Half-cell Potential method in detection of corrosion initiation and progression in RC structures.

The secondary goal of this thesis is to establish a quantitative correlation between the UGWL results and chloride contents present in the concrete specimens. This will give an insight on how the chloride-induced corrosion influence the UGWL results.

The objectives of this thesis are as follows:

- To simulate an environment of accelerated corrosion in laboratory environment.
- To compare the earliest statistically significant change in data collected by UGWL and HCP.
- To compare the advantages and limitations of the two methods (UGWL and HCP).

- To establish a quantitative correlation between UGWL data determined chloride contents, and benchmark to literature.
- To provide a recommendation for sample size in the analysis of chloride content.

1.3. Scope

The study presented in this thesis is limited in scope to:

- Reinforced concrete bridge deck structures – specimens were made using materials that are often used in bridge decks. The concrete mix used in this study was 47BD which is the typical mix used by Nebraska Department of Transportation (NDOT).
- Corrosion – deterioration of reinforcement bars as a result of chemical reactions between the steel and surrounding environment.
- Ultrasonic testing – ultrasonic guided wave leakage method will be used as the primary non-destructive testing technique to detect corrosion in reinforced concrete structures. The changes in amplitude readings obtained were used to indicate the onset and progression of corrosion.

1.4. Outline of Thesis

This thesis will describe in details the ability of ultrasonic guided wave leakage (UGWL) method in detection of corrosion, and its advantages over Half-cell potential method. Motivation, background, research goals and objectives, and the scope of the study are presented in this chapter.

Chapter 2 presents a literature review regarding corrosion-induced deterioration in reinforced concrete (RC) structures, and the non-destructive assessment techniques used in this study. It also provides a pros-and-cons study between UGWL and Half-cell potential methods.

Chapter 3 describes the experimental methodology used for laboratory concrete slabs. This chapter presents a detailed description of testing equipment used, test assemblage, various variables involved in testing.

Chapter 4 presents the results for the onset and progression of corrosion in laboratory specimens. The results reported compare the collected ultrasonic measurements to half-cell potential measurements. The results of chloride testing on concrete specimens are also presented in this chapter.

Chapter 5 points out highlights summary, conclusions, as well as recommendations resulting from this study.

CHAPTER 2

LITERATURE REVIEW

2.1 Introduction

The management and maintenance of civil infrastructures, such as bridges, is of great importance to ensure the safety of the community. Failure of bridges may cause highway network breakdown, and may result into high repair costs. Despite the ample economical and material investments in highways and roads of approximately $64.6billion, and 260 million metric tons of concrete annually, poor conditions of the roads remain a major problem in the United States (FHWA, 2002; Kelly, 1998; Kendall et al., 2008).

Dunker and Rabbat (1990) carried out a comprehensive study of highway bridge performance recorded in the American national bridge inventory (NBI) database. This study found that the percentage of structurally deficient bridges in the United States differs drastically from state to state, with the central and southeastern states having the highest deficiency percentage, and the lowest deficiency percentage was found in the southwestern states, as shown in Figure 2.1. This difference in the percentage of structural deficiency was considered to be affected more by differences in funding, design, construction, inspection, and maintenance policies rather than the climate and heavy truck-loads (Dunker and Rabbat, 1990). It was also observed that the bridge deck is the most common deficient element on interstate bridges.

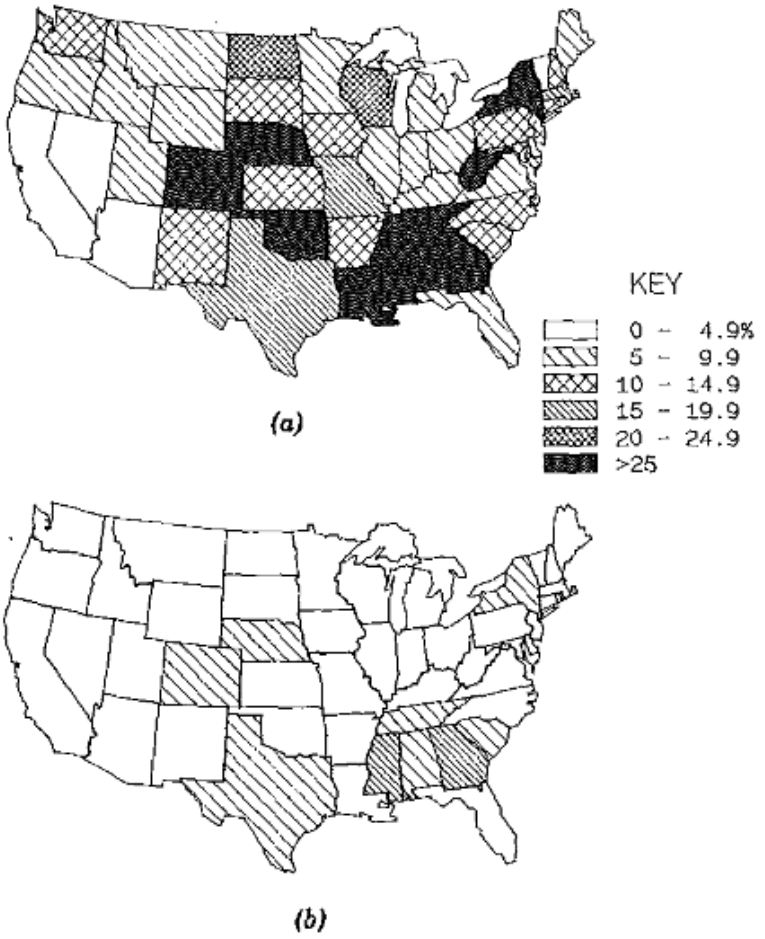

Figure 2.1 – Percentage deficiency of the bridges: (a) built 1950-1987; and (b) built 1980-1987 (Dunker and Rabbat, 1990)

A service life of 75-100 years is often expected by bridge owners for new bridges. However, it is estimated that majority of existing bridges that are only 10-20 years old are in need of expensive repair nationwide (Dunker and Rabbat, 1990; Aktan et al., 1996). Thus, life-cycle assessment, routine inspection and maintenance of roads and bridges is of major importance. Life-cycle assessment is defined as the process of assessing the environmental impacts of a facility (i.e. bridge) throughout its life cycle (Du & Karoumi, 2013). There is an

increasing demand for more accurate and cost-effective condition assessment and maintenance approaches. To evaluate bridge conditions, it is necessary to perform periodic inspections.

2.2 Bridge Inspection

It is the duty of Federal Highway Administration (FHWA) to maintain inspection consistency across the United States by implementing National Bridge Inspection Standards (NBIS). It is required by FHWA to inspect and rate the conditions of bridges and their main elements (e.g. bridge decks, superstructure, and substructure) every two years (Lounis et al., 1998). Consequently, the Departments of transportation (DOTs) are responsible to report the results of their inspection to the National Bridge Inventory (NBI). The NBI uses the data to analyze bridges and assess their conditions aimed at identifying which bridge requires maintenance, repair, or replacement.

2.3 Corrosion of Reinforcing Steel

Corrosion of reinforcing steel (rebar) in concrete is one of the most common issues that affects structural integrity and serviceability of concrete structures. The damage caused by corrosion leads to cracking, spalling, and loss of concrete cover (Mehta et al., 1993). Corrosion process in RC can cause a reduction in diameter of the rebar and debonding at the concrete-steel interface.

One of the main causes of failure of reinforced concrete structures, such as bridge decks, is cracking (El Hajj et al., 2017). Corrosion in reinforcing steel bar (rebar) in concrete structure can be one of the causes of cracking. Corrosion in RC bridge decks alone is accountable for approximately 15 percent of concrete deterioration, which is more than any other individual degradation mechanisms (Basheer et al., 1996). Although steel provides more strength to the

structure, it can also act as a source of initiation of cracking initiating because of its tendency to corrode (El Hajj et al., 2017).

Corrosion of rebar is one of the main problems in reinforced concrete structures (RC), especially when they are under the influence of chloride products and are subject to carbon dioxide (CO_2) (Tesfamariam et al., 2018). This problem leads to very high repair costs which is sometimes even more than the initial construction costs, or to the collapse of the structure in extreme conditions (Ji et al., 2013). Research shows that the repair costs of bridges in North America was approximately $23 billion in 1998. Therefore, corrosion has a great impact on the performance and serviceability of concrete.

Thus, an effective identification and/or a realistic forecasting of the onset and early stages of corrosion can significantly reduce the expenses due to maintenance, as well as prevent catastrophic hazards (Rakotovao Ravahatra et al., 2019). The study of the corrosion initiation in RC have the following advantages: (1) better knowledge of the factors leading to corrosion (Rakotovao Ravahatra et al., 2019); (2) prevention or minimization of damage due to corrosion (Winston Revie and Herbert H, 2008; Zhou et al., 2015; Rakotovao Ravahatra et al., 2019).

Further, El Hajj et al. (2017) points out that a deterioration model is required to cover three phases of deterioration process, which is the cracking process of the reinforced concrete (RC) structure. These three phases are as follows: (1) corrosion initiation due to ingress of an aggressive agent (i.e. chlorides); (2) corrosion of the reinforcement steel (rebar) and crack initiation; (3) crack propagation from the rebar to the surrounding material, i.e., concrete. When the amount of chloride on the surface of the rebar exceeds the chloride concentration limit, depassivation of the rebar occurs leading to the onset of the corrosion (El Hajj et al., 2017).

To construct a deterioration model, it is important to evaluate the time at which corrosion begin and propagate throughout the structure. Time to corrosion damage (t_{sp}) can be obtained as the sum of three phases (Bastidas-Arteaga and Stewart, 2016; Tesfamariam et al., 2018): (1) corrosion initiation (t_{ini}); (2) onset of cracking ($t_{cr,i}$, time to first cracking–hairline crack of 0.05 mm width); (3) crack propagation ($t_{cr,p}$, severe cracking in concrete). Thus, $t_{sp} = t_{ini} + t_{cr,i} + t_{cr,p}$.

Fontana (1986) describes the corrosion of steel in concrete as the reverse process of metallurgical extraction. Initially, steel is produced from oxides as the oxide ores extracted from earth undergo a metallurgical process, which is thermodynamically unstable. With production of steel, more energy is added to the system. Nature tends to revert to the lowest form of energy, and as a result, steel is reduced to the original oxides as shown in Figure 2.2.

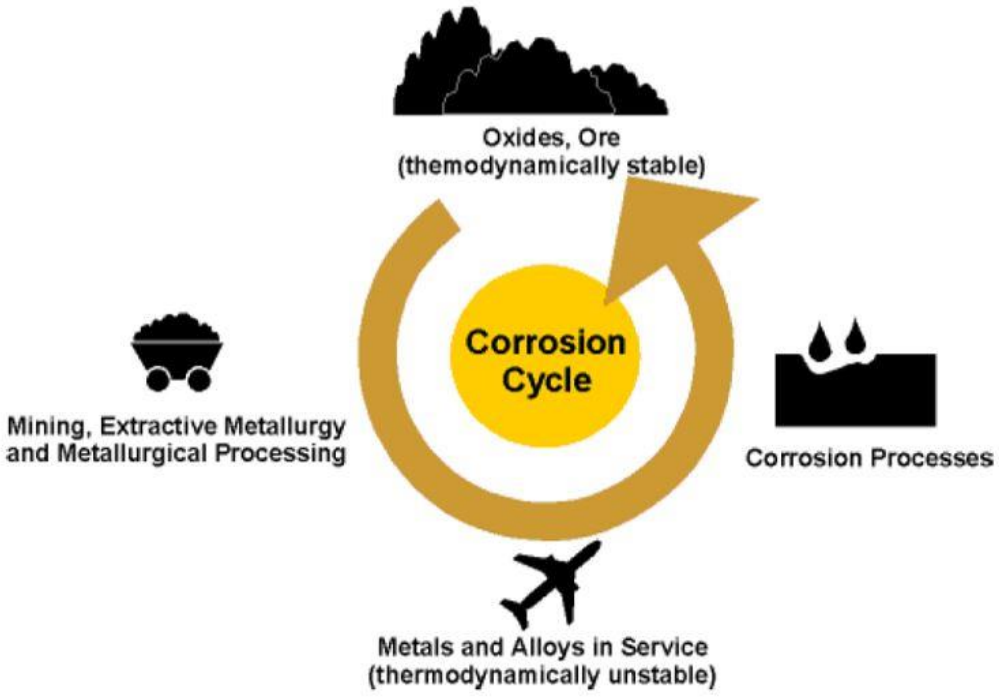

Figure 2.2 - Corrosion life cycle (Corrosion-club, 2007)

Corrosion can also be described as the chemical delamination which is a type of flaw that has not yet caused any physical separation in the concrete-steel interface (Miller, 2010). However, a chemical delamination often leads to mechanical delamination, which is the physical separation or debond of concrete-steel interface, which is when structural issues start to happen (Eric Garcia et al., 2019).

Various stages of corrosion process are illustrated in Figure 2.3. Two primary factors leading to the onset of corrosion are concrete carbonation and chlorides. Carbonation occurs when the carbon dioxide present in the atmosphere penetrates into the concrete and reacts chemically. Chlorides are present from deicing salts on the roads, seawater, chemical admixtures, and high ground salinity.

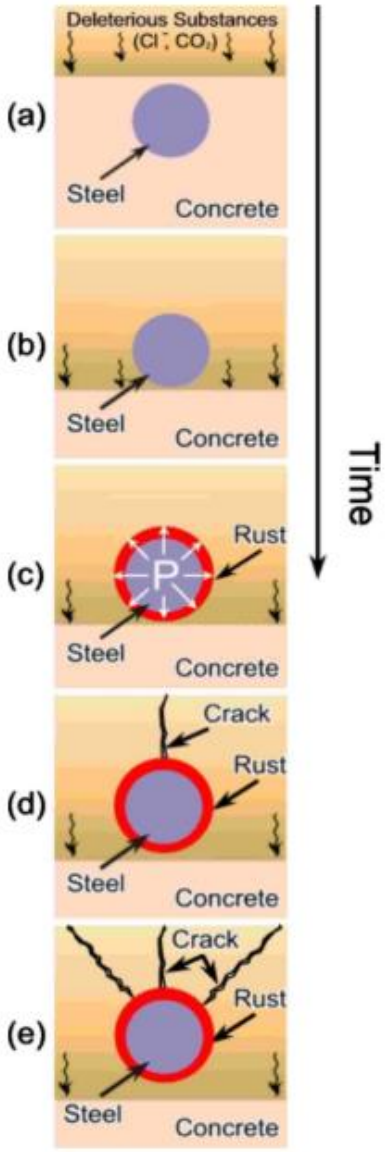

Figure 2.3 – Progressive stages of corrosion process in RC structures (Ervin et al., 2009)

Both concrete carbonation and chlorides causes the loss of the protective passive layer at the surface, as shown in Figure 2.3(b). With the presence of water and oxygen, the onset of corrosion occurs once the protective layer is destroyed (Cui, 2012; Miller, 2010; PCA, 2002). Electrochemical reactions that involve steel, water, and oxygen form a corrosion product at the rebar surface. It has been stated that the volume of corrosion products (rust) can be 2.5 – 6 times greater than the volume of steel (Karakurt & Topçu, 2012). The increase in volume creates a

pressure at the interface, see Figure 2.3(c), which causes the concrete to strain and thus the cracking begins as illustrated in Figure 2.3(d). Three mechanisms that causes deterioration are the loss of steel cross-sectional area, debonding between concrete and steel due to cracking, and the loss of concrete cross-sectional area from spalling (Ervin et al., 2009).

Corrosion in rebar can be classified into uniform corrosion and localized or pitting corrosion. Uniform corrosion is the type of corrosion in which small corrosion cells are formed over a large length of the rebar which results in an overall reduction of rebar cross-section. This type of corrosion can be detected easily. Pitting corrosion is defined as a type of corrosion in which a small portion of the rebar acts as anode due to high negative potential and rest of the rebar acts as cathode. Anodic portion undergo corrosion process and it causes a reduction in the rebar cross-section at that site (Ji et al., 2013). Low to medium amounts of chloride lead to more localized attacks, i.e., pitting corrosion, whereas medium to high amounts of chlorides and concrete carbonation causes more uniform deterioration (Ervin et al., 2009).

2.4 Corrosion Mechanism

Due to high alkaline nature of concrete, a passive layer is formed around the rebar which protects it from corrosion. The breakdown of the passive layer can lead to the initiation of corrosion. The destruction of the passive layer is mainly caused by carbonation and chloride attack. Carbonation can cause a decrease in the alkalinity of the pore liquid in concrete which results in the depassivation of the rebar, causing the corrosion process to begin (Zivica, 2003). The CO_2 gas can permeate into the concrete where it reacts with the hydration products and alters the internal structure of the concrete which results in the reduction the pH of the concrete pore solution (Liu et al., 2014).

Contrary to corrosion caused by carbonation, chloride-induced corrosion can result into severe localized damage (i.e. pitting corrosion). Additionally, chloride attacks on the concrete structures may be a result of different sources such as deicing salts, as well as from the marine environment (Peter A. Claisse, 2016). Similar to carbonation, chloride ions' attack can cause the breakdown of the passive layer of the reinforced steel, which eventually results in the onset of corrosion. These two processes (carbonation and chlorination) are shown in Figure 2.4.

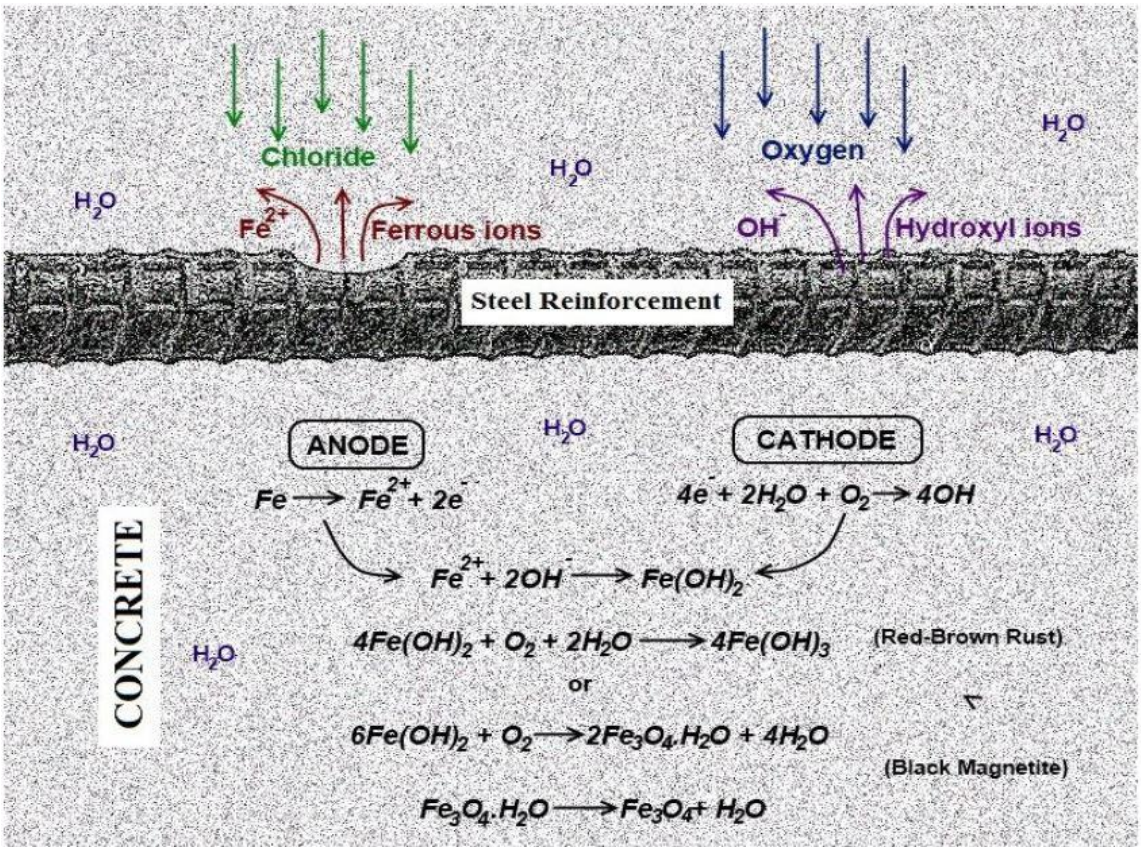

Figure 2.4 – Corrosion mechanisms in RC structures (Balakumaran, 2010)

2.4.1 Carbonation

Carbonation is defined as the process in which carbon dioxide gas in the atmosphere interact with alkaline hydroxides that are present in the concrete pore water. Carbonation is generally considered to cause depassivation and uniform corrosion of reinforcements (Balayssac & Garnier, 2017). In the first stages of construction, reinforced structures possess high alkalinity of approximately pH 12-13 because of the calcium hydroxide present in the concrete, which results into formation of a protective passive layer around the reinforcing bar (Cho et al., 2016). The pH of the concrete is influenced by the ingress of acids from outside environment (CO_2 from air or acid rain) (Aïtcin & Flatt, 2015). The passive layer protects the rebar from corroding. Nevertheless, with the penetration of carbon dioxide (CO_2) gas present in the atmosphere into the concrete, a reaction takes place between the penetrated carbon dioxide and calcium hydroxide ($Ca(OH)_2$) which results in a decrease in the pH of the concrete (Cho et al., 2016). The carbonation of the concrete is generally expressed with the following reaction that involves the reaction of calcium hydroxide to calcium carbonate:

$$Ca(OH)_2 + CO_2 \rightarrow CaCO_3 + H_2O \qquad (2\text{-}1)$$

Corrosion initiation takes place once the pH of the concrete is lowered to a value of 9 when the carbonation front (carbonation depth) has reached the steel bar beyond the concrete cover thickness (Delatte, 2009), which results in the breakdown of the protective passive layer. Rust formation is a chemical reaction which is related to temperature; therefore, in the sub-zero temperatures, the corrosion rate is lower than the areas with high temperature (+ 20–40 °C) (Delatte, 2009). Once the corrosion products are formed around the reinforcing bar, volume expansion takes place which results in the formation of cracks in the concrete surrounding the steel bar (Cho et al., 2016). The time to depassivation of the rebar is influenced by the total

amount of alkaline hydration products in concrete, and the availability of CO_2 and water (Aïtcin & Flatt, 2015).

2.4.2 Chlorination

Chloride ions may be present in the concrete when chloride-contaminated components or $CaCl_2$ are used as an accelerator in the process of mixing the concrete, or they may diffuse into the concrete from the outside environment (Wang et al., 2014). Chloride ingress causes localized breakdown of the passive layer, causing localized corrosion (pitting) in those areas. In chloride-induced corrosion, two processes occur simultaneously: (1) a repair process for the disrupted oxide layer by OH^- ions; (2) a breakdown process by chloride ions (Ahmad, 2006). Ahmad (2006) points out that chloride may be present in concrete from the following sources: (a) aggregates containing chlorides salines; (b) mixing water; (c) sea-coastal environment; (d) road de-icing salts.

Researchers also classify the sources of chloride as ‘internal’ and ‘external’ (Pradhan & Bhattacharjee, 2011): The chloride introduced to concrete at construction time (i.e. from mixing water, chloride-contaminated aggregates, chloride-contaminated admixtures) is defined as ‘internal chloride’; whereas, the chloride that enters concrete when the concrete is hardened from outside environment (i.e. us of de-icing slats on bridge decks, seawater in marine structures, from soil and ground water that contain chloride salts) is known as ‘external chloride’.

Alexander (2016) points out different transport mechanisms by which chlorides may penetrate concrete. These mechanisms are listed as follows:

1. *Diffusion* – It is defined as the mass transfer of chloride (or other) ions from areas of high concentration such as a surface exposed to seawater to the areas of low concentration (i.e. location of steel).
2. *Convection* – It is defined as the mass transfer of salt-laden water into concrete due to a moisture gradient. The movement of salt water due to moisture gradient is often described with the terms such as ‘capillary suction’ and ‘absorption’.
3. *Permeation* – It is described as the penetration of salt water due to a hydraulic gradient, where the salt water is ‘driven’ into concrete with pressure. The flow rate due to a hydraulic gradient is affected by hydraulic conductivity (or water permeability), *k*, of concrete.
4. *Migration* – It is defined as the movement of ions under an electrical gradient. In this process, negatively charged chloride cations are ‘driven’ towards the positively charged anode. The migration rate is affected by the diffusion coefficient, *D*, of the concrete and the potential gradient.

With chloride ingress in concrete, the following reactions shown in Equations 2-2 and 2-3 take place (Peter A. Claisse, 2016):

$$Fe^{++} + 2Cl^{-} \rightarrow FeCl_2 \quad (2\text{-}2)$$

$$FeCl_2 + 2H_2O \rightarrow Fe(OH)_2 + 2HCl \quad (2\text{-}3)$$

2.4.3 Methods for Quantifying Chloride Content

The determination of chloride content in concrete often involves various tasks. To determine chloride thresholds in concrete, a core may be extracted from certain locations on the test specimens after being exposed to corrosive conditions. The cores are often pulverized and

converted to powder form so that the measurement of chloride concentration is made possible. Samples that are in the pulverized form may then be used to measure chloride content. Chloride content is usually measured at the surface of the rebar or at different depths from the surface of concrete to indicate chloride ingress and the risk of corrosion at the rebar level.

Researchers use different techniques to determine chloride concentration in concrete structures. Pradhan & Bhattacharjee (2009) measured chloride levels in concrete specimens using potentiometric titration using an automatic titrator, using an equipment called *Metrohm 785 DMP Titrino* for beam specimens after being exposed to 3% sodium chloride (NaCl). Oh et al. (2003) measured free chloride threshold and OH^- threshold by ion chromatography and direct titration methods using phenolphthalein indicator. Ion chromatography was used by Meck & Sirivivatnanon (2003) for the evaluation of chloride penetration into concrete after having the concrete samples fully immersed in 3% NaCl solution.

2.4.4 Chloride Content Analyses

Determination of chloride content in the concrete or other cementitious material can be used to indicate the possibility of corrosion initiation. Corrosion process may initiate once the chloride content at the rebar level has reached certain threshold values (i.e. 0.1% by weight of cement as specified by ACI 357), where this value is often called *critical chloride content* or *chloride threshold level (CTL)* in literature (Angst et al., 2009). CTL can be defined as the minimum concentration (threshold) of chloride at the at the steel depth that has the ability to initiate the corrosion process. CTL is also defined as the amount of chloride that is required to sustain local passive layer breakdown, and initiate corrosion process (Glass & Buenfeld, 2000). The first measurement of CTL was done by Hausmann (1967). Measurement of CTL has a great importance in service life prediction in RC structures.

Generally, there are two ways of defining chloride threshold value (Schiessl & Lay, 2005; Angst et al., 2009): from a scientific standpoint, chloride threshold content can be defined as the quantity of chloride necessary for the depassivation of steel (Definition 1); and, from a practical engineering perspective, critical chloride content is the chloride content that is connected with "visible" deterioration in RC structures (Definition 2). According to (Angst et al., 2009), two different phenomena are associated with the aforementioned definitions: with the depassivation as a criterion in the Definition 1, it only takes into account the initiation stage of the corrosion process; whereas in case of Definition 2 that is related to visible or acceptable deterioration, the propagation stage of corrosion process is also considered. Practical engineering definition brings about a higher value of critical chloride content; however, Definition 1 is more precise because it indicates chloride content that is directly associated depassivation (Angst et al., 2009). Different values of chloride threshold level are given in literature.

According to (Ann & Song, 2007), chloride ingress from de-icing salts or from seawater can result in chloride content on the surface of the rebar, causing the chloride threshold level (CTL) to exceed. After the onset of corrosion, measurement of chloride content or profile to determine CTL is carried out. In general, there are two types of analyses done for chloride measurements: water-soluble and acid-soluble. Water-soluble method is used to determine the concentration of chloride using a solution obtained from boiling concrete or mortar sample in a pulverized form in water. This procedure is usually used to measure free chloride level in cementitious materials. Free chloride content can be referred to as the internal chloride that exists in the ingredients of the concrete. On the other hand, acid-soluble method is used for the estimation of the total amount which is comprised of both free and bound chlorides present in concrete. ASTM C1152 and ASTM C1218 provide guidance on the determination of acid-

soluble and water-soluble chloride contents, respectively. Bound chloride is the portion of chloride that has penetrated into the concrete from outside environment and chemically reacted or physically absorbed to the cement hydration products (Rahman et al., 2012). Acid-soluble method is the most commonly used method for determination of total chloride (Ann & Song, 2007).

2.4.5 Ion Chromatography

Ion chromatography (also known as ion-exchange chromatography) is a process in which separation of ions and polar molecules takes place. It is used for water chemistry analysis in which concentration of major ions such as fluoride, chloride, nitrate, nitrite, and sulfate, as well as major cations such as lithium, sodium, ammonium, potassium, etc., is measured. The concentrations of different ions are measured by separating them based on their interaction with a resin. The ionic concentrations in the sample are determined by the retention time of different species.

Prior to conducting a chromatography test, the liquid samples must be filtered so as to remove all the sediment and residuals. The collection of samples must be done by a sterile syringe or bottle rinsed three times with sample water. The samples must then be filtered through a 0.45um filters. A minimum sample size for the analysis is 5 mL, with no maximum limit.

After the analysis is done, the concentrations of different ions moving through the columns at a specific time will be represented by the height and breadth of the peaks, where it can be correlated to the concentrations of different ionic species present in the sample.

2.4.6 Expression of Chloride Threshold Level

Critical chloride content or chloride threshold level may be expressed in a number of ways. CTL is mostly expressed in terms of "*chloride content relative to the weight of the cement*" (Angst et al., 2009). CTL may also be expressed as total chloride content relative to the weight of concrete. Another way of expressing critical chloride content in concrete is to express CTL as a ratio of free chloride to hydroxyl threshold or $[Cl^-]:[OH^-]$ or Cl^-/OH^- (Ann & Song, 2007; Angst et al., 2009; Glass & Buenfeld, 2000); which represents the chloride ion activity to the pH of the pore solution. While Hausmann (1967) is a proponent of representation of CTL as $[Cl^-]:[OH^-]$ as pointed out by Angst et al. (2009), Page & Havdahl (1985) suggest that Cl^-/OH^- ratio is not a reliable indicator because experimentally it was found that addition of silica fume leads to an increase in Cl^-/OH^- in pore solution, but also results to higher density of microstructure which makes chloride ingress slower. Thus, a higher Cl^-/OH^- in the pore solution does not necessarily indicate the risk of corrosion initiation (Angst et al., 2009). Additionally, ratio of $[Cl^-]$: $[OH^-]$ may not be a good representation of CTL since it does not account for the inhibitive properties of cement hydration products. Inhibitive property of concrete may be defined as its ability to resist a local fall in the pH level that may otherwise results into passive layer breakdown (Glass et al., 2000). The preferred way of representing CTL is by total chloride content relative to weight of cement due to the ease in determination and because it takes into account the corrosion risk of bound chloride and the inhibitive effects of hydration products present in cement (Ann & Song, 2007).

2.4.7 Chloride Threshold Contents in Literature

There are different values for CTL in literature. A significant amount of research has been done to quantify the CTL for steel corrosion, but the estimated values are in a considerable

wide range (Ann & Song, 2007). In fact, the values of CTL ranges from 0.04 to 8.34% total chloride by weight of cement (Angst et al., 2009). This wide range of CTL values can be attributed to a number of reasons such as method of measurement, method of indication of CTL, steel-concrete interface conditions and the effect of environmental factors (Ann & Song, 2007). According to ACI 318, which provides guidance on chloride limits in concrete, the CTL is in the range of 0.05 to 0.1% by weight of concrete. These limits are also provided by Technology in Practice (TIP) (NRMCA: Technology in Practice). According to British Standard, the limits of chloride content for RC structures and pre-stressed concrete structures are given as 0.4% and 0.1% respectively. The calculated CTL for bridges in United Kingdom ranges between 0.2 and 1.5% by weight of cement indicated as total chloride content (Ann & Song, 2007). Table 2.2 indicate the chloride threshold levels given by different standards.

Table 2.2 – CTL specified by different standards

Standard	**Chloride Threshold Level (CTL) (%,cement)**	
	Reinforced Concrete	Pre-stressed Concrete
British Standard	0.4	0.1
European Standard	0.2 – 0.4	0.1 – 0.2
ACI 357 (Water-soluble Cl^-)	0.1	0.06
ASTM 1152 & ACI 222 (Acid-soluble Cl^-)	0.2	0.08

2.5 Accelerating Corrosion

To study corrosion behavior in RC structures, researchers create an environment with corrosive conditions. One of the means to accelerate corrosion is to immerse RC slabs in NaCl solution. According to literature, different concentrations of NaCl has been used.

Yuan et al. (2009) measured corrosion current density of steel bar in concrete under a designed artificially controlled climate environment. Two different ways were used to accelerate the corrosion in RC slabs. The first set of specimens were immersed in 10% NaCl solution, and the second set of specimens were cast with 5% cement weight of NaCl. It is stated that the corrosion process exhibits the characteristics of the time-variant corrosion rate. The researchers illustrated three phases of the corrosion process. In the first phase, a decrease in the corrosion rate is observed. This phase is followed by a steady state phase in which the corrosion rate remains in a steady state for some time. Finally, an ascending phase of corrosion rate is observed after the corrosion caused concrete cracking to occur. The results from the first set of specimens (immersed in 10% NaCl solution) indicated a descending phase at first, and then the rate of decent decreases. The rate remains in a steady state after almost 100 days. Finally, the rate starts ascending as a result of concrete cracking after almost 150 days. The results from the second set of specimens (cast with 5% NaCl) indicate a decrease in the corrosion rate which lasts about 21 days. A steady phase is followed after the descending phase. Finally, the current density starts ascending after almost 70 days.

It was observed by Yuan et al. (2009) that the corrosion process in the second set of specimens was shorter than the first set of specimen were concrete specimens were immersed in 10% NaCl solution.

Abbas et al. (2014) conducted a rapid Cl^- penetrability test to investigate the effects of Cl^- in precast concrete tunnel lining (PCTL) segments by conducting different tests. Five specimens having 100 mm (4 in.) diameter and 50 mm (2 in.) thickness were tested. The cores were extracted after 90 days of exposure to corrosive conditions to determine the chloride content for these specimens. The results indicate that the specimen immersed in 10% NaCl solution showed higher chloride level (% by weight of concrete) of approximately 0.4% at the depth of 5 mm (0.2 in.) as compared to RC specimen immersed in 3.5% NaCl solution that showed 0.12% of chloride level at the same depth.

2.6 Corrosion Monitoring Methods

Various structural issues threatening the safety and serviceability of concrete structures, as well as the high repair and rehabilitation costs due to these problems have led to development of non-destructive testing (NDT) techniques. The most commonly used evaluation technique by Departments of transportation (DOTs) in the U.S. to evaluate the bridge decks structural integrity are qualitative methods such as visual inspection, hammer sounding, and chain dragging because they are inexpensive and easy-to-use. With recent advancement in testing techniques, NDT methods such as ground penetrating radar (GPR), ultrasonic pulse velocity (UPV), and impact echo (IE) have also been used for evaluation of concrete structures. These methods which have the potential to provide quantitative information about the bridge decks conditions, are the most effective evaluation techniques when used together (Clemeña et al., 2000; Cui, 2012; Gucunski & Council, 2013). However, these methods are still not often used by DOTs because they are more expensive and time consuming compared to qualitative methods.

2.6.1 Ultrasonic Testing

The ultrasonic pulse-velocity (UPV) tests were first developed in the 1940s using a device known as a Soniscope (Manning, 1985). This instrument was then designed to be much smaller and more suitable for field applications. The previous soniscopes were heavy and labor intensive, while modern soniscopes or ultrasonic testing devices are smaller, portable, and battery-operated (Manning, 1985).

The vibration frequencies are generated by electronic pulses. Then, a transducer converts these frequencies into mechanical energy. Though higher frequencies have higher sensitivity to smaller defects, and can be used with the specimens having lesser thicknesses, they are also subject to higher attenuation (Manning, D. G., 1985). Furthermore, Ervin (2007) used both low and high ultrasonic frequencies to monitor corrosion. For detection of cracks in concrete structures, lower ultrasonic frequencies are used due to the inhomogeneity of concrete. In general, the vibration frequencies used in ultrasonic testing are usually in the range of 20 to 150 kHz to detect flaws (i.e. delamination, corrosion, and cracking) in concrete, while frequencies of 150 kHz have only been utilized in laboratory studies (Manning, D. G., 1985; Bindal, V. N. et al., 2003; Yaman, I. O. et al., 2000).

Ultrasonic testing involves two types of transducers: transmitting, and receiving. Both transducers are attached to surface of the test specimen at certain distances apart from one another. The electronic pulses are generated by the transmitting transducer (transmitter) and collected at the receiving transducer (receiver), and the travel time between the transmitter and receiver is measured electronically (Manning, D. G., 1985).

Figure 2.5 illustrates three ways of attaching the transmitter and receiver to the area of inspection. In the direct-transmission method, the receiver is coupled to one of the specimen, and the receiver is attached to the other end. This arrangement provides highest sensitivity compared to other attachment options (i.e. semi-direct transmission and surface transmission).

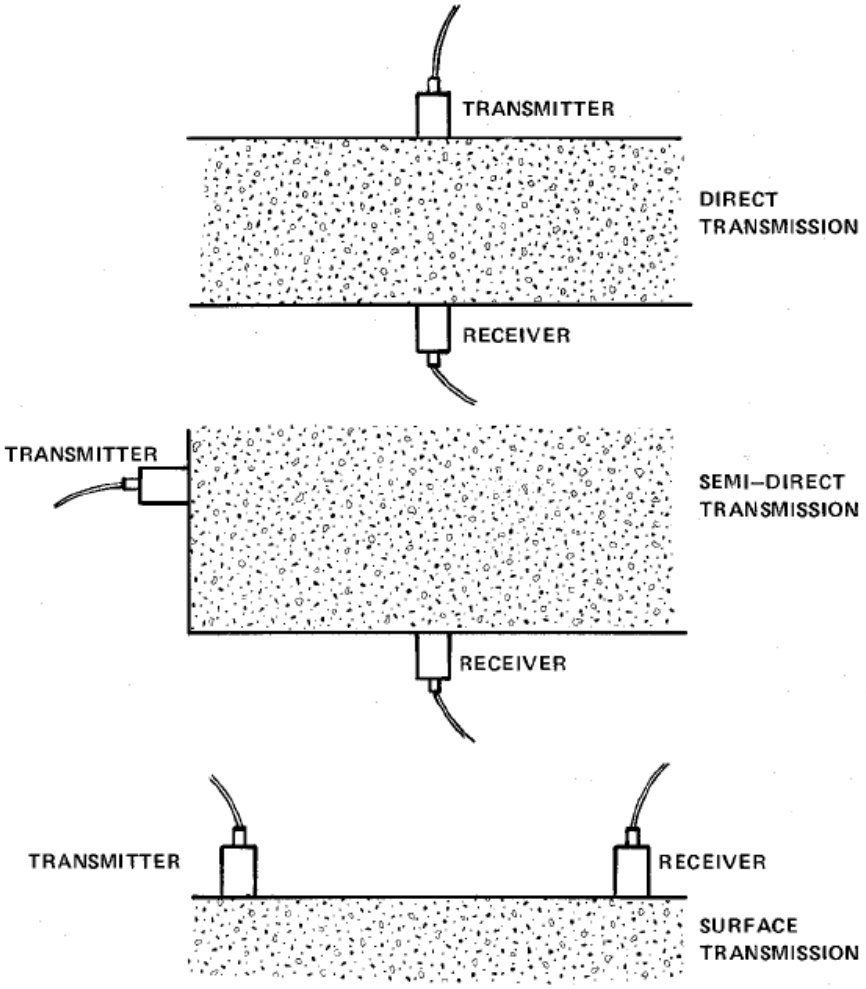

Figure 2.5 – Methods of measuring pulse velocity (Manning, D. G., 1985)

Semi-direct transmission and surface methods are used when it is not possible to use direct-transmission for the area to be inspected. Bridge decks typically fall into this category.

Lastly, in the surface transmission method, both the transmitter and receiver are placed on the surface. This method provides information on the quality of the concrete near the surface only.

The accuracy of pulse-velocity measurements may be influenced by various factors such as the smoothness of the concrete surface, concrete temperature, moisture content, mixture proportions, and concrete age (Manning, D. G., 1985). Smoothness of the surface can significantly influence the coupling conditions and accuracy of the readings. Figure 2.6 shows some of the factors that influence the transmission of ultrasonic waves in concrete.

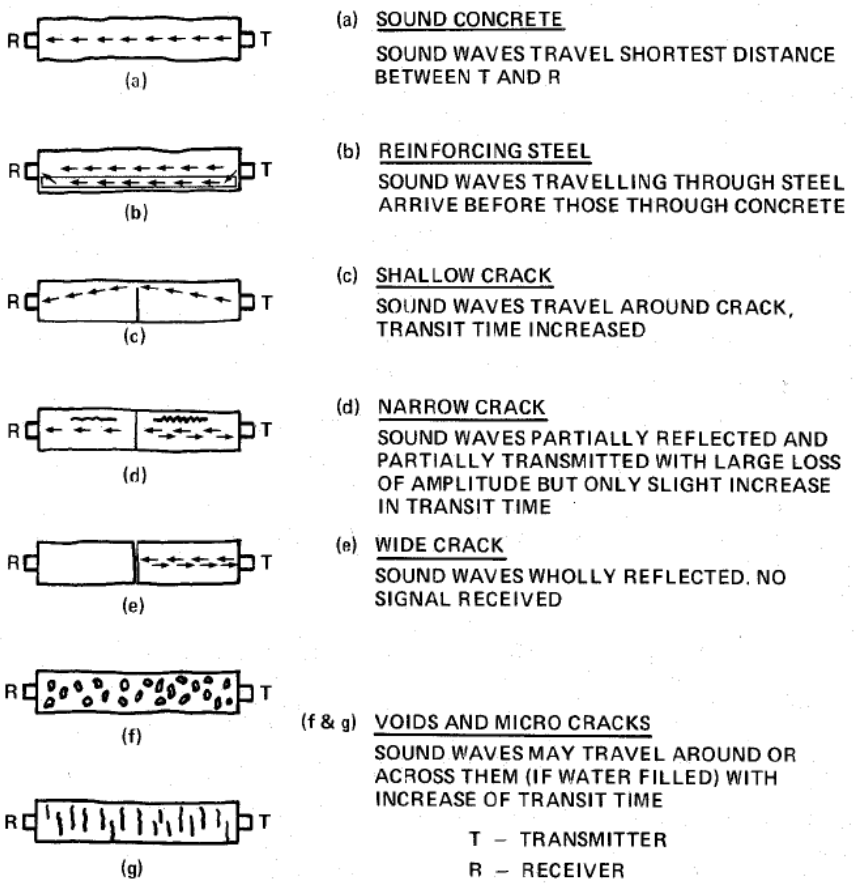

Figure 2.6 – Factors affecting the transmission of ultrasonic waves in concrete (Manning, D. G., 1985)

2.6.1.1 Ultrasonic Wave Propagation

Typical applications are illustrated in Figure 2.7. “Pulse-echo” and “through transmission” techniques are shown in Figures 2.7(a) and 2.7(b) respectively. These methods are used to monitor the condition of a structure by recording the signals propagating through the specimens. Variations in the collected measurements can indicate the onset of flaws at an inspected region. The “pulse echo” and “through transmission” techniques are often used to perform C-scans. C-scan is an image created by plotting the data collected from an ultrasonic testing, and are basically shown in plan views. C-scans are used to measure point by point a desired area of inspection, and provides information on how the properties of waves across the inspected area change. The information is provided usually in terms of time of arrival, phase velocity, or amplitude of the signals.

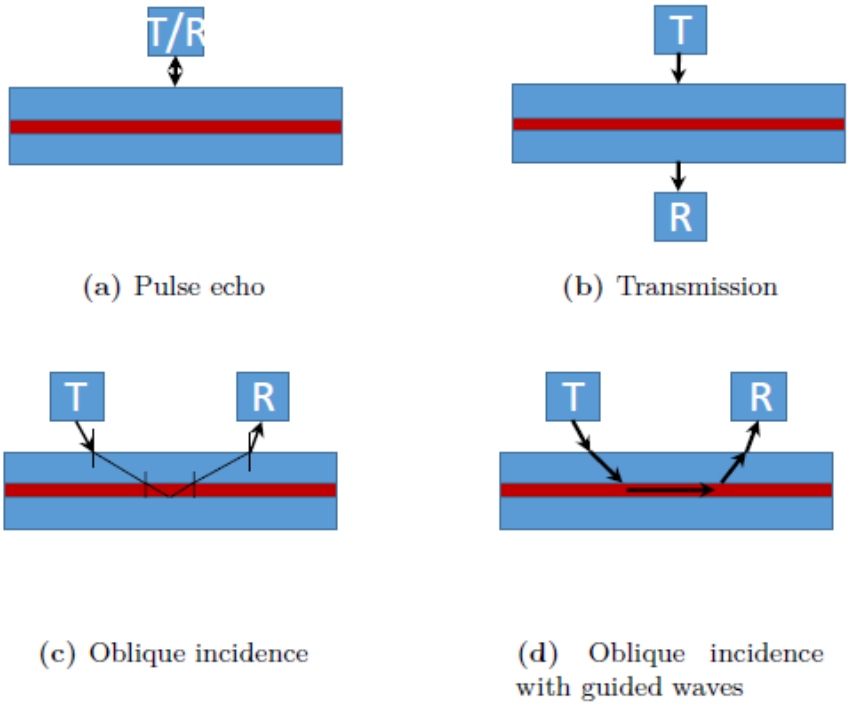

(a) Pulse echo

(b) Transmission

(c) Oblique incidence

(d) Oblique incidence with guided waves

Figure 2.7 – Common ultrasonic adhesive bond inspection techniques (Rose, 2002)

Figure 2.7(c) illustrates “oblique incidence” in which the signals propagate at an angle. The main advantage of this method is that this method is more practical for field application as only access to the top surface is needed.

Finally, Figure 2.7(d) refers to the oblique incidence technique with guided waves. In this technique, the ultrasonic waves are generated in the specimens by transmitting the energy through the waveguide, i.e., steel embedded in concrete. Part of this energy gets leaked out into the surrounding material (i.e. concrete). Several studies have demonstrated the ability of UGW to identify debonding of steel-concrete interface (Li et al., 2012; Miller, 2010; Garcia et al., 2017 & 2019; Mustapha et al., 2014). These studies observed an increase in the amplitude measurements as the debond of steel-concrete interface increased.

Ultrasonic testing uses sound energy that propagate in two modes: longitudinal waves and shear waves. In Longitudinal Waves (P-waves), particle motion is in the same direction as the direction of wave propagation. However, in shear waves (S-waves), particle motion is perpendicular to the direction of wave propagation, as shown in Figure 2.8.

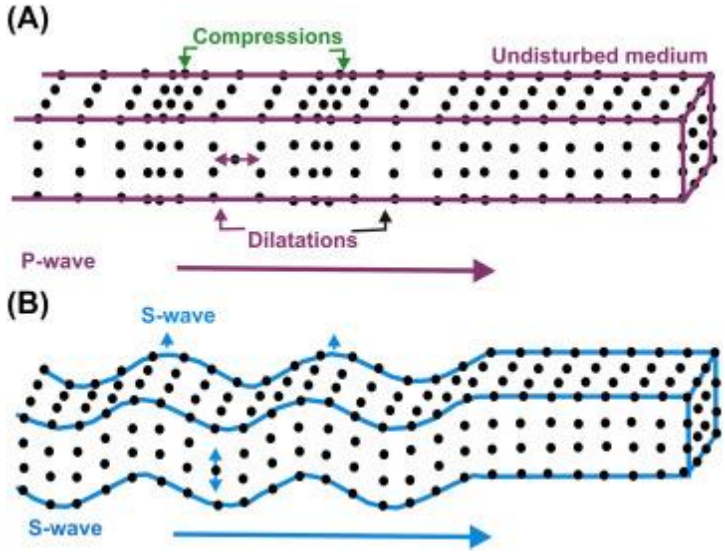

Figure 2.8 – Longitudinal and shear waves (Haldar, 2018)

Ultrasonic testing uses elastic waves that can propagate as bulk waves or guided waves (Garcia, 2016). An elastic wave is defined as a wave that propagates by the elastic deformation of a medium. Elastic wave can either propagates in a solid, liquid, or gaseous medium. Figure 2.9 illustrates bulk waves propagation in traditional UT method. In this method, the energy gets leaked out into the surrounding material and the insonified area is limited to the contact point.

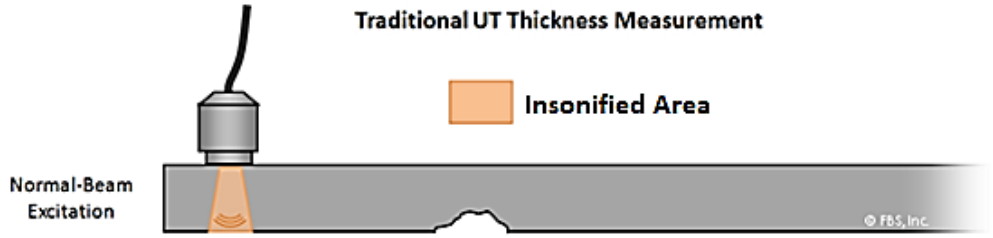

Figure 2.9 – Bulk wave propagation (Rose J. L., 2011)

Elastic waves can also propagate as guided waves through a waveguide, i.e., steel embedded in concrete as shown in Figure 2.10. The insonified area is much larger in case of guided wave propagation as the waves propagation longer distances compared to bulk wave propagation, making it a less time consuming and more cost-effective method.

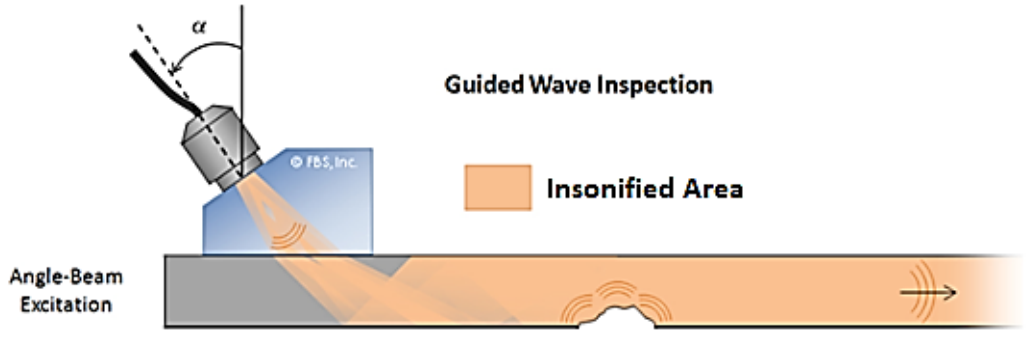

Figure 2.10– Guided wave propagation (Rose J. L., 2011)

2.6.1.2 Theory of Guided Wave

Let us consider a hollow cylinder with an internal radius *a*, thickness of *h*, and ratio of thickness to internal radius ratio of h/a as shown in Figure 2.11.

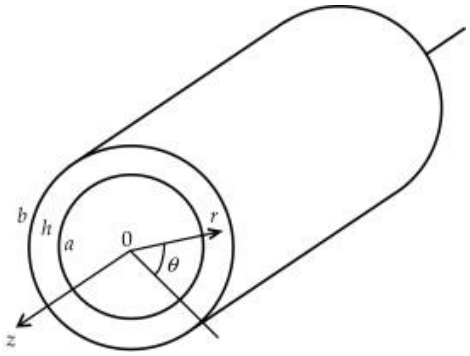

Figure 2.11 – Hollow cylinder in cylindrical coordinates (Giurgiutiu , 2014)

The propagation of energy in a body with the help of the movement of the particles can be expressed as wave propagation (Sriramadasu et al., 2019). When an elastic wave propagates through a cylindrical waveguide, it generates various modes. The governing equation of wave propagation in circular cylinders is obtained by Helmholtz decomposition of Navier's equation of motion as shown below:

$$\mu\nabla u + (\lambda + \mu)\nabla\nabla.u = \rho\left(\frac{\partial^2 u}{\partial t^2}\right) \tag{2-4}$$

where u is is the displacement vector, ρ is the density, λ and μ are Lamé constants. are Lamé constants (also known as are Lamé parameters) are two material-dependent quantities that are related to the stress-strain relationships in the materials. Generally, λ (Mu) and μ (Lambda) are also known as Lamé's first constant and Lamé's second constant, respectively. λ represents

rigidity, whereas μ is referred to as incompressibility of a material (Goodway, 2001). Additionally, in fluid dynamics, μ is referred to as dynamic viscosity of the fluid.

There are three different mode families in ultrasonic guided wave: (1) longitudinal, (2) torsional, and (3) flexural modes. At high frequencies, these modes are highly dispersive. The solution provided by Gazis for the above governing equation is considered to be satisfied for longitudinal waves (Gazis, 1959). An alternative solution that was suggested by Sun et al. (2005) holds good for both longitudinal as well as torsional modes. According to the Helmholtz decomposition, the vector *u* can be expressed in terms of a dilatational scalar potential ϕ and an equi-voluminal vector potential *H*. *u* can be expressed in terms of *H* and ϕ as:

$$\begin{aligned} u &= \nabla\phi + \nabla \times H \\ \nabla \cdot H &= F(r,t) \end{aligned} \tag{2-5}$$

The following equation, where ∇^2 is the three-dimensional Laplace operator, is obtained from substituting Equation 2-5 into Equation 2-4:

$$\nabla\left[\left(\lambda+2\mu\right)\nabla^2\phi-\rho\left(\frac{\partial^2\phi}{\partial t^2}\right)\right]+\nabla\times\left[\mu\nabla^2 H-\rho\left(\frac{\partial^2 H}{\partial t^2}\right)\right]=0 \tag{2-6}$$

According to Amjad et al. (2015), the displacement equation of motion is fulfilled if the potentials ϕ and H hold good for the wave equations:

$$v_1^2\nabla^2\phi=\frac{\partial^2\phi}{\partial t^2} \tag{2-7}$$

$$v_2^2\nabla^2 H=\frac{\partial^2 H}{\partial t^2} \tag{2-8}$$

$$v_1^2 = \frac{(\lambda + 2\mu)}{\rho} \tag{2-9}$$

$$v_2^2 = \frac{\mu}{\rho} \tag{2-10}$$

where v_1 and v_2 are bulk velocities of longitudinal and shear waves, respectively, and are expressed as following:

$$v_1 = \sqrt{\frac{(\lambda + 2\mu)}{\rho}} \tag{2-11}$$

$$v_2 = \sqrt{\frac{\mu}{\rho}} \tag{2-12}$$

The wave equations can be mathematically expressed in terms of cylindrical coordinates. A cylindrical coordinate system is a three-dimensional coordinate system in which the location of a point in the space can be described with respect to a reference axis. The general solution to the wave equations that was suggested by Sun et al. (2005) are as follows:

$$\phi = f(r)e^{im\theta}e^{i(kz-wt)} \tag{2-13}$$

$$H_\theta = h_\theta(r)e^{im\theta}e^{i(kz-wt)} \tag{2-14}$$

$$H_r = h_r(r)e^{im\theta}e^{i(kz-wt)} \tag{2-15}$$

$$H_z = h_z(r)e^{im\theta}e^{i(kz-wt)} \tag{2-16}$$

where $f(r)$, $h_\theta(r)$, $h_r(r)$ and $h_z(r)$ are potentials, m is circumferential order number, and k is wave number. From Equation 2-5, the displacement components can be expressed in terms of ϕ and H as follows:

$$u_r = \frac{\partial \phi}{\partial r} + \frac{1}{r}\frac{\partial H_z}{\partial \theta} - \frac{\partial H_\theta}{\partial z} \tag{2-17}$$

$$u_\theta = \frac{1}{r}\frac{\partial \phi}{\partial \theta} + \frac{\partial H_r}{\partial z} - \frac{\partial H_z}{\partial r} \tag{2-18}$$

$$u_z = \frac{\partial \phi}{\partial z} + \frac{1}{r}\frac{\partial (rH_\theta)}{\partial z} - \frac{1}{r}\frac{\partial H_r}{\partial \theta} \tag{2-19}$$

By applying the stress-strain relations, the stress field on the cylindrical surface is expressed as:

$$\sigma_{rr} = \lambda \nabla^2 \phi + 2\mu \varepsilon_{rr} \tag{2-20}$$

$$\sigma_{rz} = 2\mu \varepsilon_{rz} \tag{2-21}$$

$$\sigma_{r\theta} = 2\mu \varepsilon_{r\theta} \tag{2-22}$$

where the stress-displacement relationships are given as follows:

$$\sigma_{rr} = \frac{\partial u_r}{\partial r} \tag{2-23}$$

$$\sigma_{rz} = \frac{1}{2}\left[\frac{\partial u_r}{\partial z} + \frac{\partial u_z}{\partial r}\right] \tag{2-24}$$

$$\sigma_{r\theta} = \frac{1}{2}\left[r\frac{\partial}{\partial r}\left(\frac{u_\theta}{r}\right) + \frac{1}{r}\frac{\partial u_r}{\partial \theta}\right] \tag{2-25}$$

A system of homogeneous equations is given by the traction-free boundary condition on the cylindrical surface as follows:

$$[D]\{A\} = 0 \tag{2-26}$$

where D represents displacement and stresses and A relates to unknown coefficients. $[D]$ is a 3×3 matrix for a solid cylinder, and a 6×6 matrix for a hollow cylinder. These equations can be solved when the following condition is fulfilled by vanishing the determinant of the matrix:

$$Det[D] = 0 \tag{2-27}$$

The above equation is known as 'characteristic dispersion equation' (Amjad et al., 2015), and the roots of this equation provides the dispersion curves for different modes in wave propagation. By numerically solving the Equation 2-27, the dispersion relationship between wave number k and frequency ω can be obtained (Rose 1999).

Finally, phase velocity and group velocity dispersion curves can be calculated with the Equations 2-28 and 2-29 as follows:

$$c_p = \frac{\omega}{k} \tag{2-28}$$

$$c_g = \frac{d\omega}{dk} \tag{2-29}$$

2.6.1.3 Ultrasonic Guided Wave Leakage (UGWL) Method

Recently, a new ultrasonic testing method called, "*Ultrasonic Guided Wave Leakage*" was developed at the University of Nebraska-Lincoln by Garcia et al. (2017). This method is

capable of detecting the onset of various flaws in RC structures such as bridge decks. It was successfully demonstrated that this newly-developed method has the ability to identify the onset of delamination with widths as small as 0.2 mm (0.008 inches). In this method, the steel bar is used as a waveguide, and the energy is transmitted by a sensor attached to the rebar, and received by a sensor placed on desired locations on the test specimens. The study done by Garcia et al. (2019) demonstrated that the amplitude of leaked waves that radiates from the steel bar waveguide is sensitive to corrosion initiation and cracks. In their research, two different sets of RC specimens were cast for the assessment of corrosion and cracking. The first set of concrete specimens that measured 45.7 x 30.5 x 12.7 cm (18 x 12 x 5 in.) were cast with 5% NaCl solution to accelerate corrosion as shown in Figure 2.12. A #5 rebar was embedded at the center level, placed 6.3 cm (2.5 in.) from the top surface of concrete. These specimens were also submerged in the water to a depth just below the rebar. Measurements for corrosion monitoring were taken over a period of 40 days, and data was collected every 2 days. Measurements of the leaked energy using receivers on the concrete surface successfully identified the onset of various flaws such as corrosion, delamination, and cracking (Garcia et al., 2019).

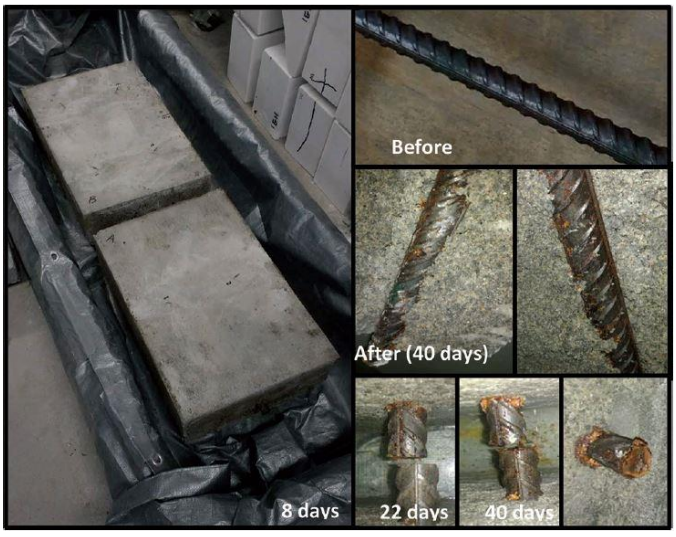

Figure 2.12 – Corrosion specimens (Eric Garcia et al., 2019)

Garcia et al. (2019) demonstrated that the signal amplitude increases as the time of exposure of concrete specimens to corrosive conditions increases. It was observed that the amount energy leaked out from the guided waves increases as the corrosion progresses as shown in Figure 2.13. It was concluded that the energy measurements are sensitive to the onset of corrosion, and hence, UGWL method can be used for detection of the corrosion initiation and progress in RC structures such as bridge decks.

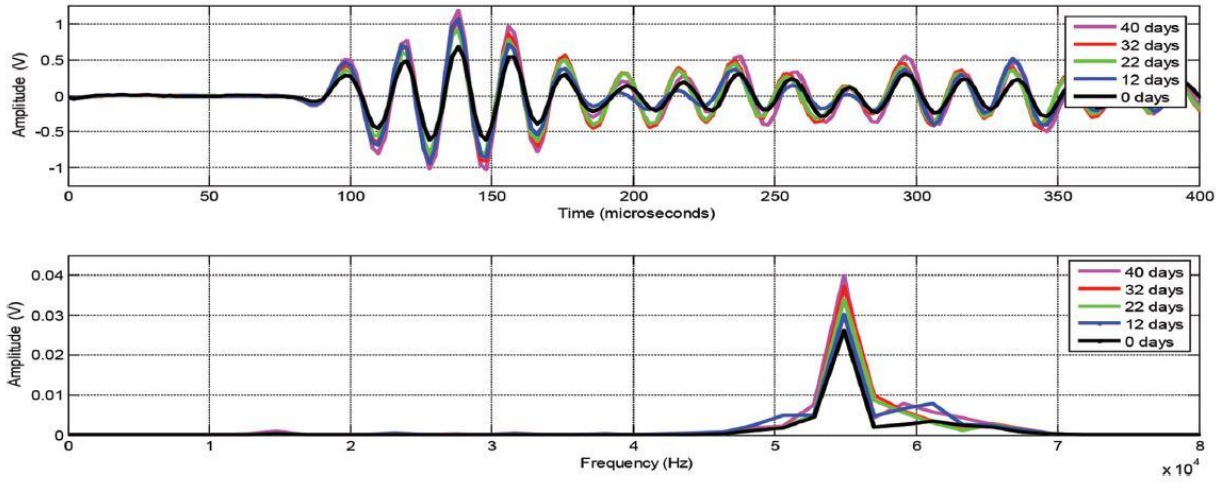

Figure 2.13 – Amplitude data indicating corrosion progression (Garcia et al., 2019)

One of the common limitations that exists in ultrasonic testing is attenuation which limits the extent to which an area is tested. Attenuation in ultrasonic testing of RC structures can be classified into two main categories (Garcia, 2016): intrinsic and geometric effects, and the recently developed UGWL technique is influenced by both.

Erdogmus et al. (2020) successfully demonstrated that UGWL method has the ability to identify multiple flaws, i.e., delamination and corrosion, occurring at different spots along the same rebar using a single setup. The authors achieved a detection range up to 427 cm (14 ft.) in a single test set up. For finding relatively accurate location of flaws, a grid of sensors located every

15 cm (6 in.) along the steel bar is recommended. Figure 2.14 shows the UGWL test set-up that was used by the Erdogmus et al. (2020), in which a transmitter is attached to one end of the rebar, and the leaked ultrasonic energy was recorded using an array of receiver on the surface of the concrete along the rebar.

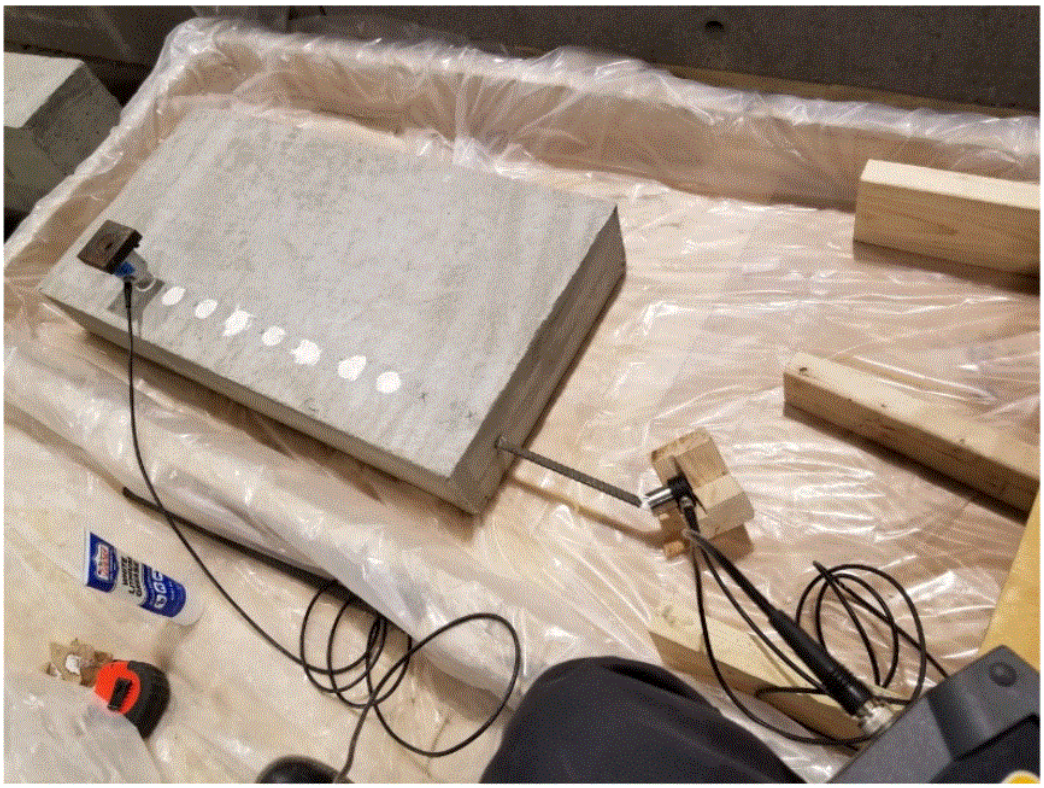

Figure 2.14 – UGWL test set-up (Erdogmus et al., 2020)

2.6.2 Half-cell Potential Method

Half-cell potentials is rapid and cost-effective way used to detect the existence of active corrosion non-destructively. Half-cell potential (HCP) Method was first used by Stratfull (1957) as a corrosion assessment method. This method can be employed to characterize the electro-chemical behavior of corrosion in the rebar. HCP measurements can be used for rebar corrosion monitoring in concrete bridge decks and other structures such as pipelines. HCP method can be used any time throughout the life of structure, regardless of the type of the environment, as long

as the temperature is more than +2°C (Elsener et al., 2003). In general, a copper/copper sulfate electrode (Cu/CuSO4) or a silver/silver chloride electrode (Ag/AgCl), usually known as 'reference electrode' is utilized for half-cell measurements, as shown in Figure 2.15. A reference electrode, which has a stable electrode potential, is also known as 'indicator electrode' that has some characteristic, which allows the potential of the other half-cell to be determined. This reference electrode is placed on the concrete surface above the rebar, and is connected to the rebar.

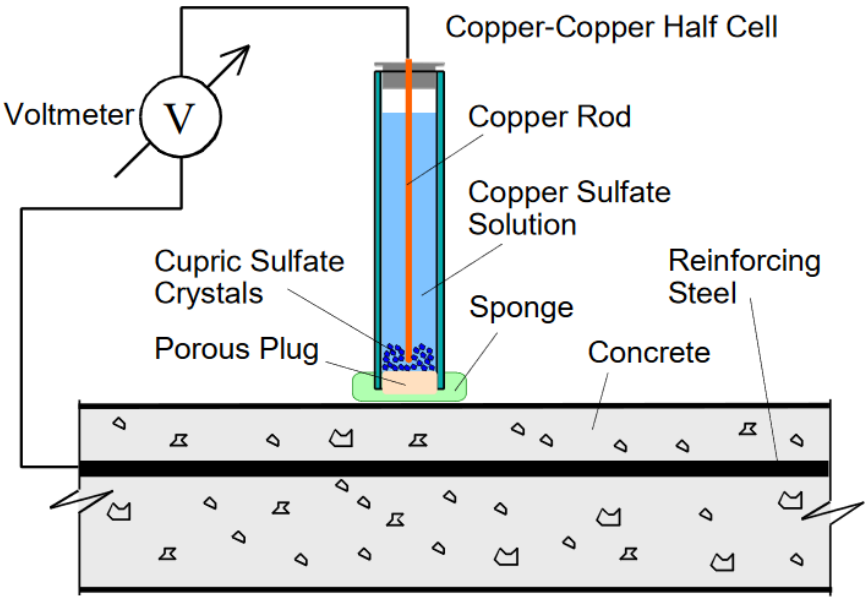

Figure 2.15 – Half-cell test set-up (Zemajtis, 1998)

ASTM C876 provides a guideline on how to conduct the half-cell measurements, and the relationship between the potential measurements and the corrosion probability, shown in Table 2.3. More negative half-cell readings indicate greater likelihood of corrosion.

Table 2.3 – ASTM C876 for interpretation of half-cell measurements

Half-cell potential measurements (mV)	Probability of rebar corrosion activity
>-200	Less than 10%
-200 to -350	Uncertain
<-350	More than 90%

According to Stratfull (1973), when relating the half-cell potential measurements to concrete cracking, the following must be noted:

1. The half-cell potential measurements of the rebar can only be statistically related to presence of cracks in concrete.
2. The half-cell potential of the rebar does not take into account the physical or structural properties of the concrete.
3. The existence of corrosion-induced cracks in concrete is related to concrete strength, absorption, moisture content, stresses, and the concrete cover.

Acknowledging the fact that half-cell potential method is a relatively easy testing technique, there are some limitations associated with this method. One of the limitations of the Half-cell potential testing method is that there is no information of the potentials between –200 and –350 mV. Frølund et al. (2003) investigated the advantages and disadvantages of half-cell potential technique. Four different on-site cases were used to assess the applicability of this method. The first case involved a bridge pillar exposed to deicing salts, and results obtained showed that there was a good correlation between corrosion rate and half-cell potential method. The second was a dry structure where half-cell potentials measurements were found to be directly misleading, while the results obtained using corrosion rate were shown to be reliable. In the third case, a wet structure was monitored, and the half-cell potential results were shown not to be a reliable representation of corrosion activity. In the fourth case, an underground parking

garage with leaking water/de-icing salts from the above street was tested. The half-cell potential measurements showed high risk of corrosion, whereas the corrosion rate was shown to be lower.

It was concluded by Frølund et al. (2003) that assessment of corrosion by traditional half-cell potential method using the current standards may result in mistakes in scenarios where concrete is water-saturated, carbonated, and exposed to very low temperature. From four presented cases of on-site measurements, three of them show the need to use another technique alongside half-cell potential for the reliability of results.

Another disadvantage of half-cell potential method is that it cannot be used for the assessment of structures involving an epoxy-coated rebar as the ASTM C876 Standard explicitly indicates that this technique is not suitable for the measurements that involve epoxy-coated steel reinforcement.

2.6.3 Comparison between the proposed UGWL and HCP Methods

A comparison is made between UGWL and HCP methods, as shown in Table 2.4. Further investigations in this thesis will address some of the advantages of the UGWL method over Half-cell potential technique.

Table 2.4 – Comparison between UGWL and Half-cell Potential Methods

Parameters	UT	HCP
Application for other purposes	Can be used to detect cracks and delamination in RC structures (Garcia et al., 2019); It can characterize material's composition, elastic properties, density and geometry (Helal et al., 2015)	Does not have other known applications other than corrosion detection
Influence of temperature	No information	Influenced by temperature and humidity (Akhtar, 2013)

Need for coupling material	It needs coupling gel (i.e. couplant) between the sensors and the test materials (i.e. concrete)	It does not need any coupling gel
Applicability on structures involving epoxy-coated bar	It was used for structures involving Epoxy-coated rebar (Garcia et al., 2017)	Not suitable for structures that involves epoxy-coated rebar (ASTM C876)
Attachment to the rebar	It requires an attachment to the rebar	It requires an attachment to the rebar

CHAPTER 3

METHODOLOGY

3.1 Ultrasonic Guided Wave Experimental Set-up

The experimental set-up used to collect the UGWL data in this project is shown in Figure 3.1. The experimental set-up is comprised of two transducers from CONTROLS-Group: 1) a 50 kHz transmitter (T), and 2) a 50 kHz receiver (R), both having the diameter of 1.18 in. (3 cm). The PULSONIC Ultrasonic Pulse Analyzer 58-E4900 from CONTROLS-Group was used as the data acquisition system to generate the ultrasonic signals and collect the measured data.

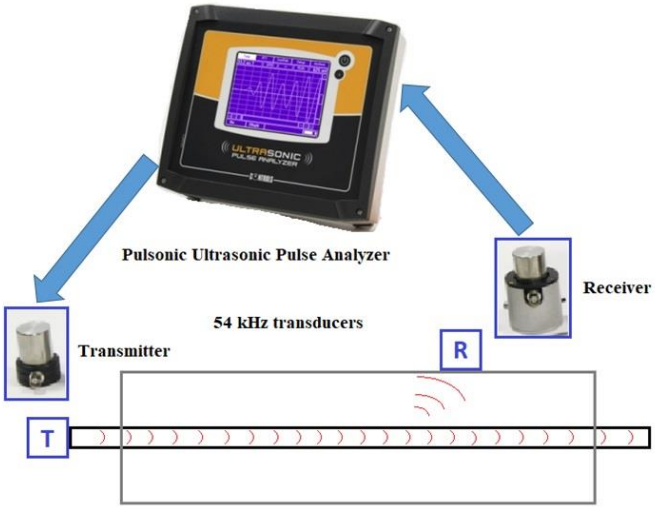

Figure 3.1 – Experimental set-up for ultrasonic testing

These piezoelectric transducers covert the electrical energy to mechanical energy and vice versa. The core of a typical piezoelectric transducer is made of a piezoelectric material which is based on the phenomenon of conversion of structural vibrations to electrical outputs. With the application of pressure, piezoelectric materials generate electricity. This pressure leads to an alteration in the polarity of the dipoles; as a result, an imbalance between the two surfaces

occurs where the two ends become polarized (Waqar et al., 2015).

In order to collect data, the transmitter and receiver were attached onto the rebar and concrete, respectively, using a couplant. While the transmitter was coupled onto the steel throughout the testing period [see Figure 3.2 (a)], the receiver was moved to monitor several equally spaced spots on the surface of the reinforced concrete specimen as shown in Figure 3.2 (b). The desired locations on the surface of the concrete were marked to locate the receiver on the same position in each testing period.

a) b)

Figure 3.2 – Sensors used to collect ultrasonic data: (a) transmitter, and (b) receiver

Couplants – A couplant is a material that helps the transmission of ultrasonic energy from the transducer into the test specimen, in this case the reinforced concrete structures. Because of the existing acoustic impedance mismatch between air and solid (i.e. such as concrete), a great amount of ultrasonic energy is reflected. The couplant is used to get more energy into the test specimen by displacing the air.

Erdogmus et al. (2020) compared two types of couplents: (1) Ultragel II from Magnaflux; and (2) White Lithium Grease from Lucas Oil Products Inc. The findings suggested that Ultragel II has a sglightly more efficiency for the purpose of trasmittting the ultrasonic energy into the system and receving the leaked energy that leak from the testing material (i.e. reinforced concrete). In this research, Ultragel II was used.

3.2 Half-cell Potential Experimental Set-up

Giatech ICOR is an NDT device that was utilized to collect measurements for half-cell potential. The experimental set-up for this testing procedure is illustrated in Figure 3.3, where a reference electrode (R) is conntected to the rebar, and the ICOR device, designated as (I), is placed on different test spots on concrete surface. This device is comprised of six corrosion measurement electrodes, one half-cell potential measurement electrode, and one temperature measurement inlet. In this method, the equipment is connected to a mobile device such as a tablet via Bluetooth where the collected data are directly stored. For each test specimen, five spots where tested on top of the concrete surface above the rebar. These locations were 6 in. apart.

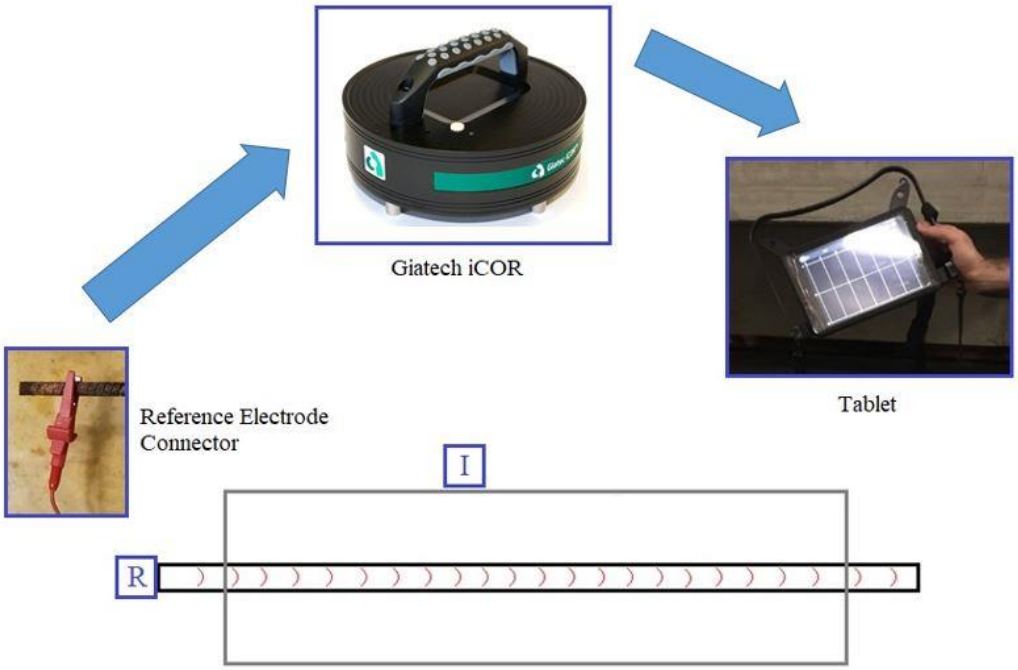

Figure 3.3 – Experimental set-up for ICOR

3.3 Materials

The concrete mix design used for laboratory specimens was 47BD, recommended by Nebraska Department of Transportation (NDOT). This concrete mix design is often used by NDOT on the bridge decks in Nebraska, and it meets the criteria specified by the American Association of State Highway and Transportation Officials (AASHTO). The properties of concrete are indicated in Table 3.1. The steel bar used in concrete lab specimens was #4 conventional rebar (0.5-inch diameter).

Table 3.1 – Properties of 47BD Mix Design used by NDOT

Designation	**Total Cementitious Material Min. (lb/cy)**	**Total Aggregate (lb/cy)**	**Air Content range (%)**	**Maximum Water/ Cement Ratio (lb/lb)**	**Minimum Required Strength (ksi)**
AASHTO Bridge Specification	611	1.0-No.4	6±1.5	0.49	4.00
47BD NDOT	658	1.0-No.4	6.0-8.5	0.42	4.00

3.4 Specimen Details

Reinforced concrete slabs of 91.4cm x 45.7cm x 12.7cm (36 x 18 x 5 in.) were cast with a No. 4 rebar (12.7mm diameter) embedded at the center of the cross-section of the slabs as shown in Figure 3.4. The rebar was projected at both ends, allowing the transmitter to be located and attached on the end of the rebar. Three replicates of RC slab test specimens were used, with each one having a different bar end angle: 0-degree; 33-degree; and 45-degree, cut with reference to vertical axis (see Figure 3.5). The purpose of cutting the end of the bars in diffenet angles was to investigate the amount of energy transfer through the rebar with different bar end angles. The signals are sent from 0-angle, as well as the angled ends, and received by the receiver on the concrete surfeace.

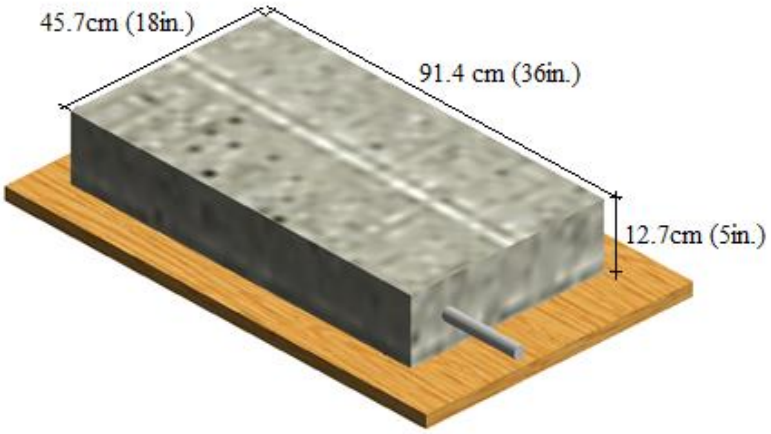

Figure 3.4 – Test specimen

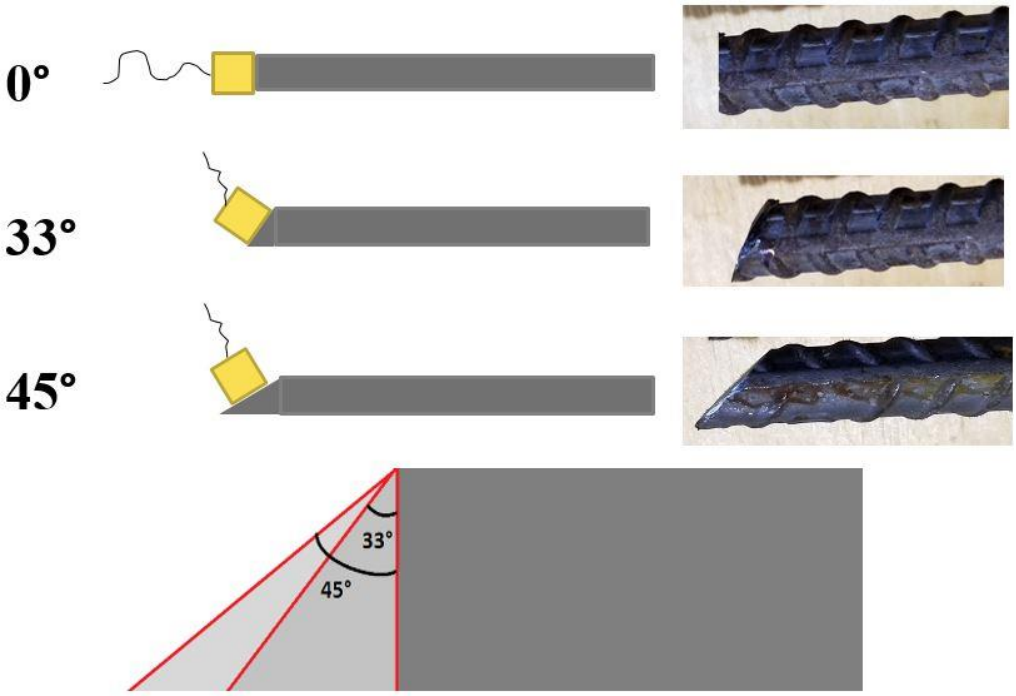

Figure 3.5 – bar end angles with reference to vertical axis (Erdogmus et al., 2020)

3.5 Inducing Corrosion

According to literature, different concentrations of NaCl have been used by researchers to accelerate corrosion in RC structures. John et al. (1981) fully immersed reinforced concrete cubes

in 3% and 10% NaCl solution to accelerate corrosion. To accelerate corrosion in RC structures, 10% NaCl concenration has also been used by (Yuan et al., 2009; Abbas et al., 2014; Wheat & Eliezer, 1985). Therefore, 10% NaCl concetration was selected over 5% concentration which is typically used to accelerate corrosoin to make the acceleration process faster.

Testified by these precedent in the literature, in this research, the concrete slabs were immersed in 10% NaCl solution. A No. 4 rebar was also immersed beside one of the test specimens to undergo corrosion as shown in Figure 3.6. Small plastic shims were placed beneath the concrete slabs to allow for the passage of NaCl solution under these specimens. A piece of lumber was placed inside the formwork to act as a water barrier to restrict the flow of NaCl to a smaller part in the formwork. During each testing period, this piece of wood was taken out so that the water level is dropped, allowing for the transmitter to be attached and coupled to the end of the rebar.

Figure 3.6 – Test specimen submerged inside 10% NaCl solution

3.6 Data Collection

For ultrasonic measurements, ten equally-spaced locations were selected and marked on the surface of the test specimens along the rebar. These test spots were 7.6 cm (3 in.) apart, with the first sport starting at 15.2 cm (6 in.) from the edge of specimen [see Figure 3.7 (a)]. For collection of half-cell potential measurements, 5 spots that were 15.2 cm (6 in.) apart where selected and tested in a similar approach to that of ultrasonic measurements as illustrated in Figure 3.7 (b). The data were collected once every 3 days for the first month. After observing the slow rate of corrosion progression, it was then decided to take measurements once every 6 days. For UGWL mehod, measurements collected from monitoring corrosion are presented as amplitude values where an change in these values indicate corrosion progression in the test specimen.

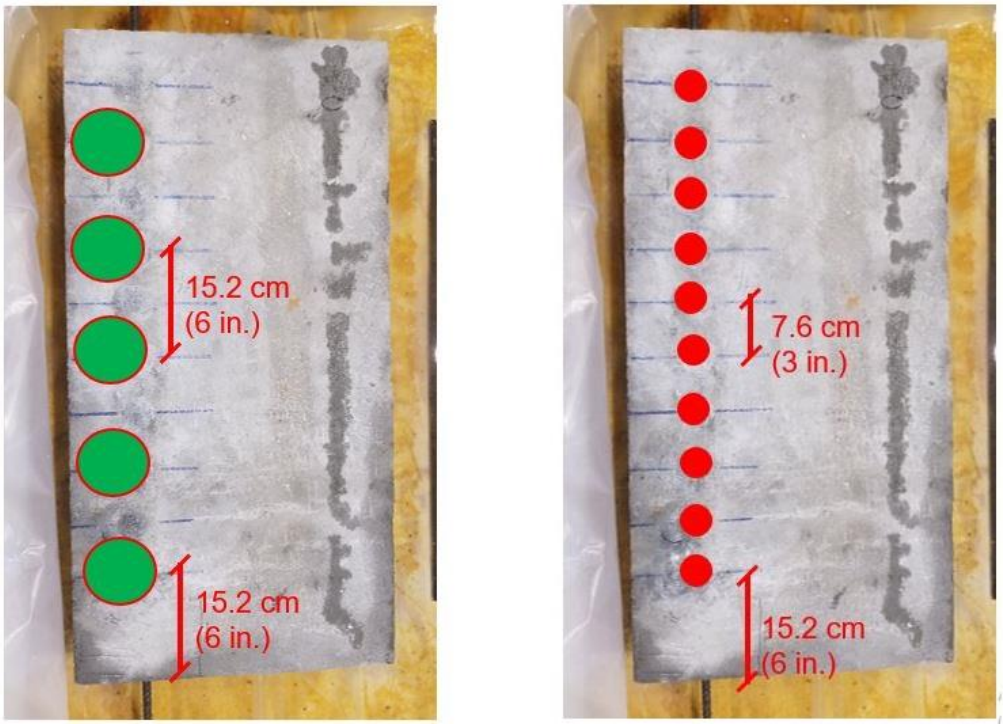

Figure 3.7 – Test spots on test specimens: (a) UGWL; (b) ICOR

3.7 Bar End Angles

The tertiary goal of this research is to make improvements to the UGWL method. Therefore, the feasibility of attaching the transmitter using angled transducer wedges on the rebar in bridge decks in order to direct more of the longitudinal waves into the rebar. Since the end of the rebar is not exposed in real life situaiton, a different approach such as tapping process must be adopted. To further explore the amount of energy transmission with different bar end angles, the concrete slabs were cast with rebars with different bar end angls: i.e. 0-degree; 33-degree; and 45-degree, cut with reference to vertical axis as shown in Figure 3.5.

3.8 Measurement of Chloride Content

After the laboratory specimens were monitored for corrosion using UGWL and Half-cell potential methods, chloride content was determined in 0-degree specimen to correlate chloride content present in concrete to the collected measurements by UGWL and Half-cell potential. For this purpose, two test spots were selected for analysis of chloride content. 0-degree specimen was cored on two locations to the rebar level as shown in Figure 3.8. The extracted cores were then broken into smaller pieces, and got pulverized to achieve a powder form suitable for chloride analysis (see Figure 3.9).

Figure 3.8 – Extracted cores from the concrete specimen

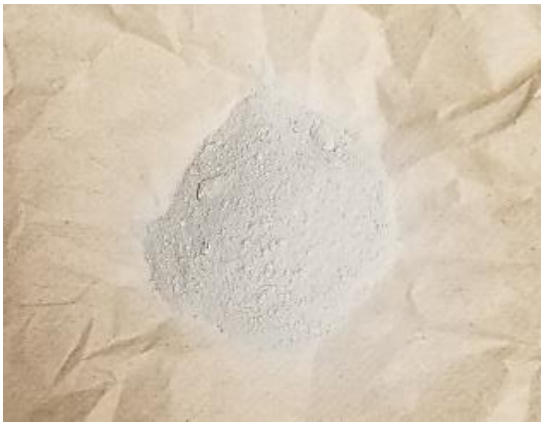

Figure 3.9 – Concrete sample in pulverized form

The concrete samples were then passed through No. 20 sieve (850 μm) as recommended by the ASTM C1152 that provides guidance on acid-soluble test to determine chloride content. After the sieving was done, the samples were mixed properly to get homogenized. To run the analysis, approximately 2 gm of each sample was taken and mixed with 5 mL of nitric acid, as well as Methyl Orange Indicator inside beakers. After observing a pink color for the samples, the samples were kept on a heat plate until the samples start boiling, as shown in Figure 3.10.

Figure 3.10 – Concrete samples on the heat plate

After the solutions reached the boiling point, they were filtered through filter paper inside flasks (see Figure 3.11) using filter paper so that any residuals or particulate matters do not interfere with the solution.

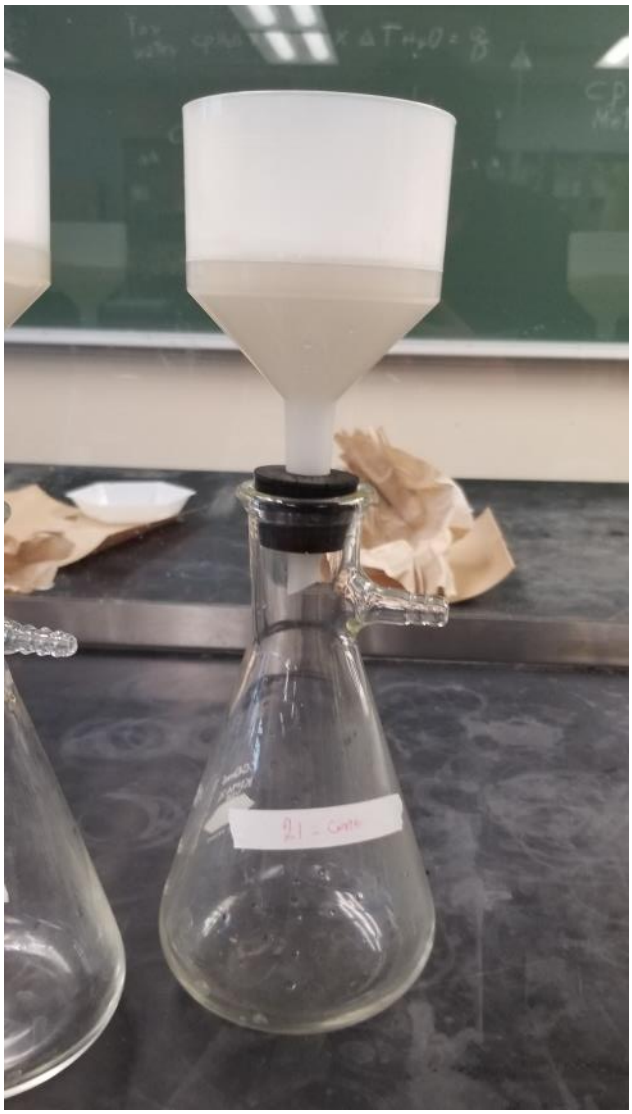

Figure 3.11 – Filtering the samples using filter paper

After filtering the samples, the final solution was prepared inside volumetric flasks with 250 mL of purified water as shown in Figure 3.12. The purified water was used for filtering as well so that more reliable results are achieved in chloride content analysis.

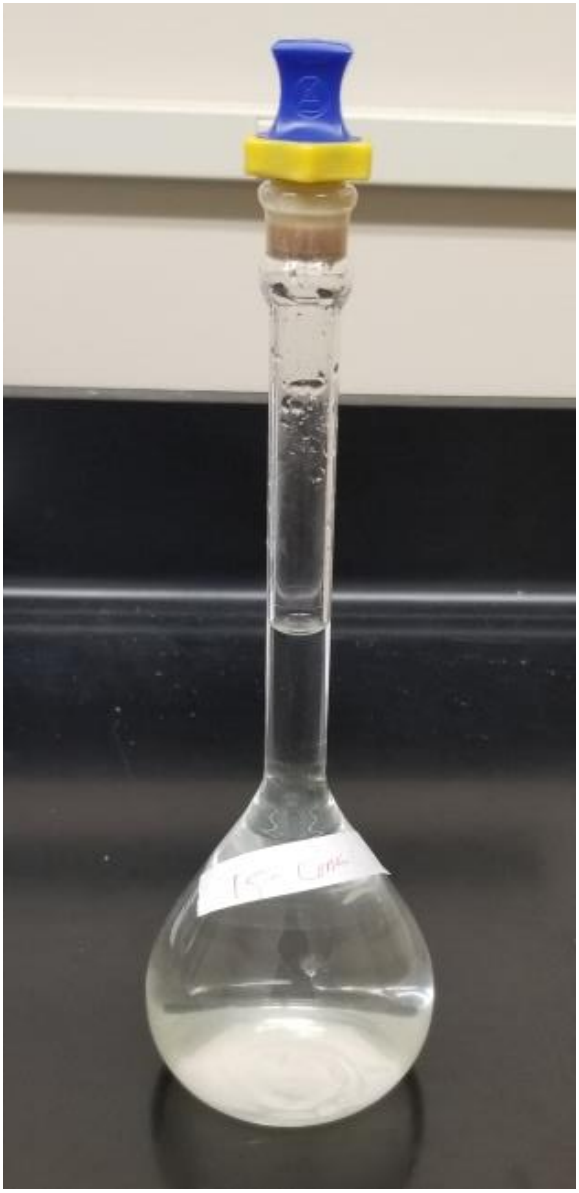

Figure 3.12 – Samples prepared for ion chromatography analysis

After preparation of the samples accoridng to ASTM C1152, the ion chromatography testing was conducted using Eco IC Chromatography System from Metrohm shown in Figure 3.13. Each sample was tested using this equipment to determine the concentrations for different ionic species such as fluoride, chloride, nitrate, nitrite, and sulfate.The goal for this experiment was to determine the total chloride level present in the concrete samples, and the results of this experiment are presented in Chapter 4 of this thesis.

Figure 3.13 – Eco IC Chromatography System from Metrohm

CHAPTER 4

EXPERIMENTAL RESULTS

The experimental results presented in this chapter are aimed to achieve three specific objectives: (1) to demonstrate the advantages of the recently-developed UGWL method over the traditional Half-cell Potential measurements in detection of the onset and progression of corrosion; (2) to determine chloride content present in the concrete specimens after being exposed to corrosive environment, and; (3) to establish a correlation between the chloride contents and measurements done by UGWL and HCP methods. Prior to accelerating the corrosion, baseline data were collected using UGWL. However, in case of HCP method, the measurements were taken after the specimens were immersed in NaCl solution.

4.1 Monitoring Corrosion Using UGWL

The purpose of the experiment was to monitor the progression of corrosion in the laboratory test specimens. Figures 4.1 – 4.3 present sample time and amplitude plots for 0-degree specimen for days 3, 6 and 9 versus the baseline data. Figure 4.4 show a combined plot for Figures 4.1 – 4.3. Prior to taking the measurements for corrosion build-up, the other errors caused by irregularities on the concrete surface were minimized. In order to do that, sandpaper was used to smoothen the test spots right above the rebar on the surface of the concrete. According to previous findings (Garcia et al., 2017; Garcia et al., 2019), an increase in the measured amplitude values indicate corrosion onset and progression. Based on this prior information on indication of corrosion initiation and progression, corrosion was detected starting with Day 9 of the process as illustrated in Figure 4.3 and 4.4. Further increase in the amplitude values was observed with time, and the measured data on Day 30 of corrosion provide a clearer

indication of corrosion progression, as shown in Figure 4.6. It was also observed that the first few points are more sensitive; hence, the difference between the amplitude values are more obvious because the distance between the transducer and receiver is less for these locations. As the distance along the rebar increases, the amplitude values seem to be close. It is because the guided waves start to attenuate more as the distance between the transmitter and receiver increases, whereas in case of the data obtained for the test spots for which the distance between the transmitter and receiver is less, the attenuation is less.

The exponential attenuation of amplitude readings of the leaked energy along the length of specimen is demonstrated using an envelope that is shown by two theoretical curves, as shown in the plots representing the UGWL readings in this chapter. Garcia (2016) previously determined the limits of the envelope by assuming a high attenuation coefficient and then a low attenuation coefficient. It was observed that the dimensions of the specimen tested could affect the measurements. With a smaller dimension of the specimen, it is more likely that the reflection within the concrete would be detected by sensors, which would result in larger increases of the higher amplitude measurements at the starting end of the guided wave, and therefore, use of a higher attenuation coefficient is more appropriate. The smaller specimen used by Garcia (2016) measured 45.7cm x 45.7cm x 12.7cm (18 in. x 18 in. x 5 in.) demonstrated higher attenuation coefficient. The lower bound (blue dashed line) demonstrated in the following plots is the highest attenuation coefficient obtained, which was found to be 0.052. The larger specimen measured 168cm x 45.7cm x 12.7cm (66 in. x 18 in. x 5 in.), however, showed lower attenuation compared to the smaller specimen. The upper limit (red dashed line) is the attenuation coefficient, which was obtained from the leaked waves in specimens of larger dimensions, and as expected, shows the same attenuation as the guided wave itself. The larger specimen was further

tested with different arrays of the sensors. The arrays located at greater distances from the rebar showed attenuation coefficient similar to the guided wave attenuation, whereas the arrays located at closer distances from the steel bar showed higher attenuation. This was attributed to the fact that the surrounding boundaries are much closer to the rebar, resulting in early detection of reflected waves, which gradually attenuates with distance. Arrays located 6.3cm (2.5 in.) and 7.6cm (3 in.) away from the rebar resulted in higher attenuation compared to the arrays that were 31cm (12.25 in.) and 38cm (15 in.) far from the rebar. In this research, with the specimens measured 91.4cm x 45.7cm x 12.7cm (36 x 18 x 5 in.), and since the distance of the receiver to the rebar is 6.35cm (2.5 in.), it is more likely that the attenuation coefficient is similar to that of the smaller specimen obtained by Garcia (2016). It can also be observed from the following plots that the majority of the data is closer to the lower bound, which represents higher attenuation coefficient.

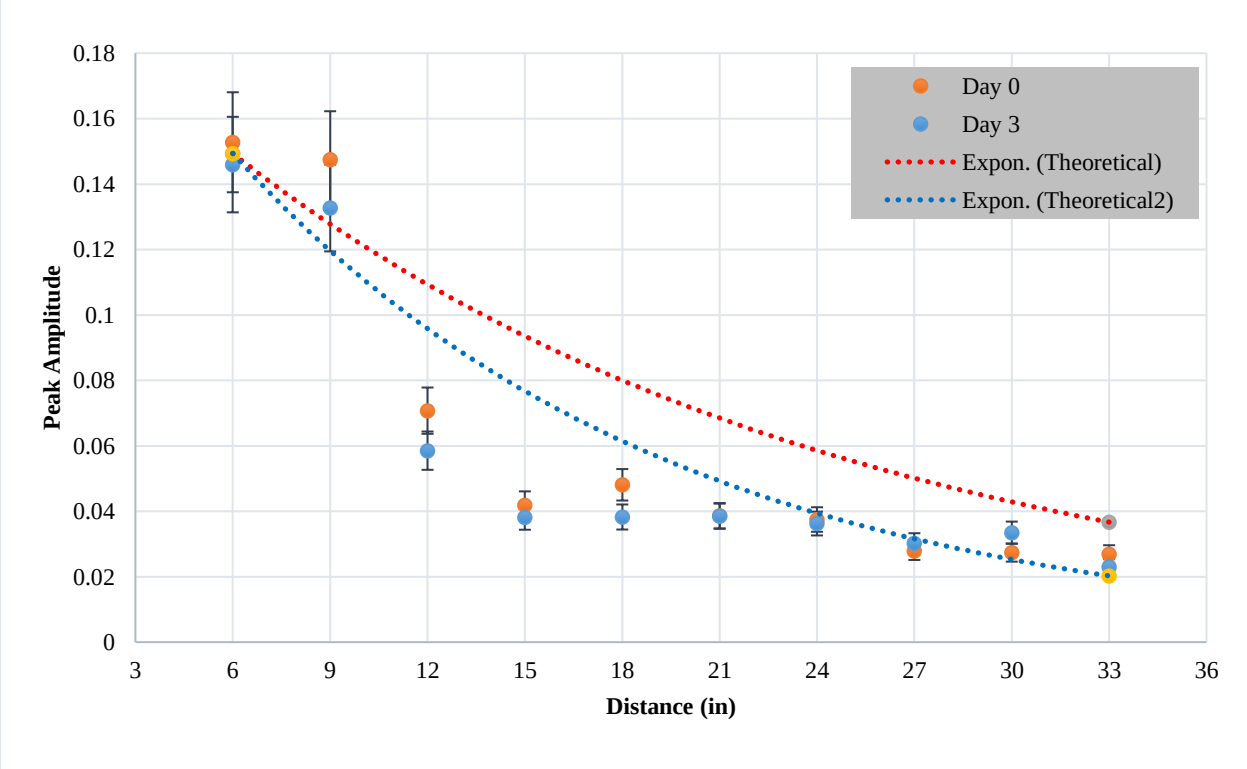

Figure 4.1 – Day 0 versus Day 3 Corrosion in 0-degree specimen

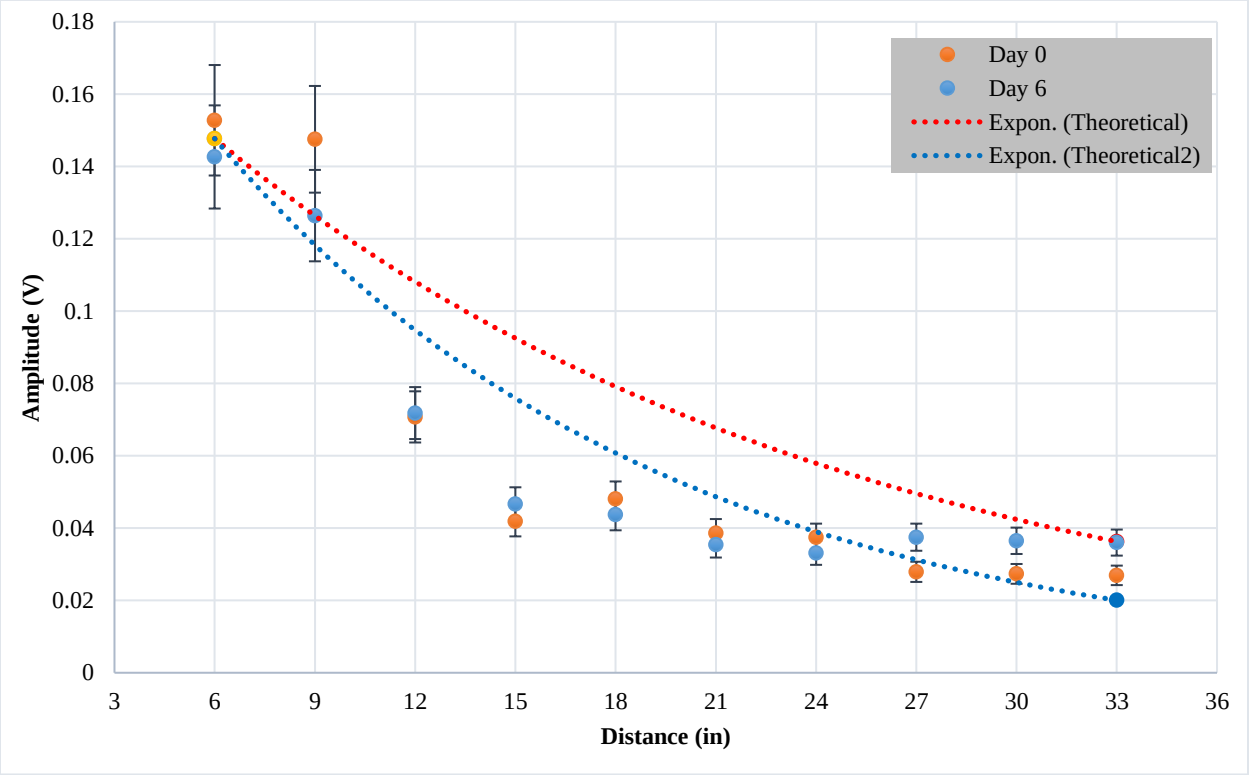

Figure 4.2 – Day 0 versus Day 6 Corrosion in 0-degree Specimen

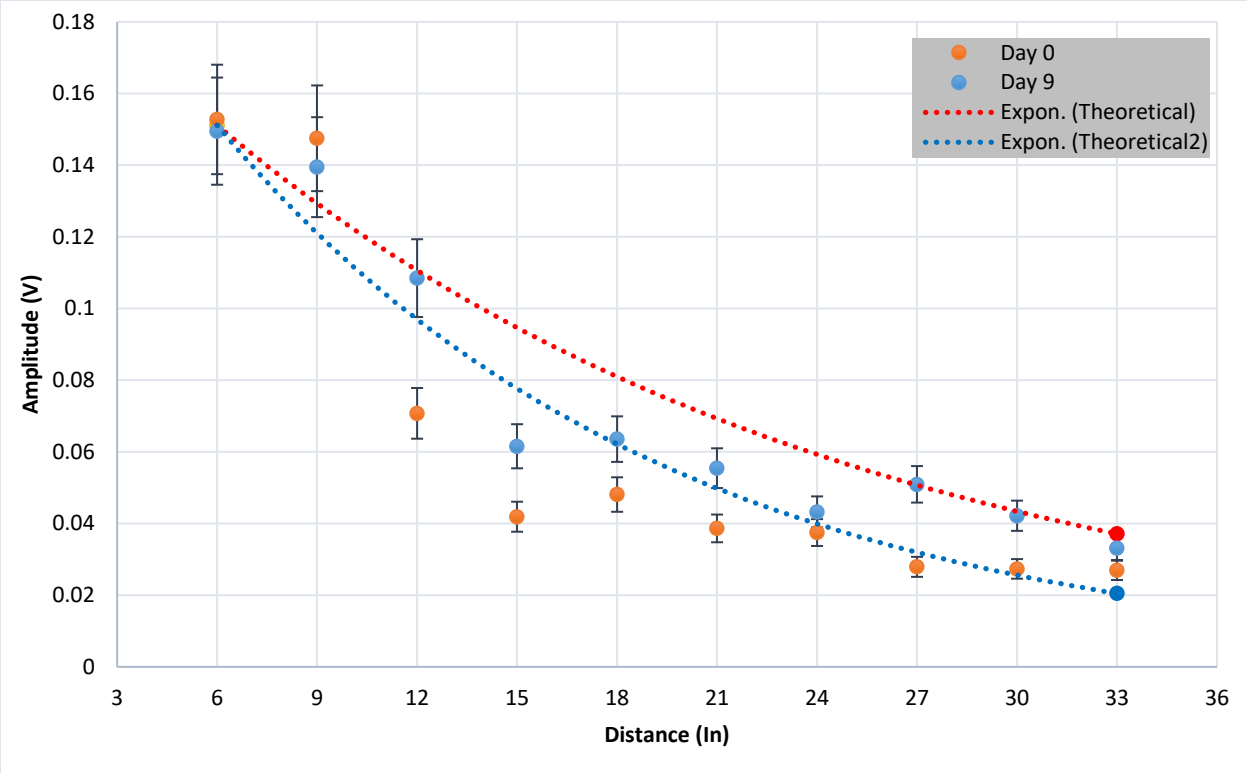

Figure 4.3 – Day 0 versus Day 9 Corrosion in 0-degree Specimen

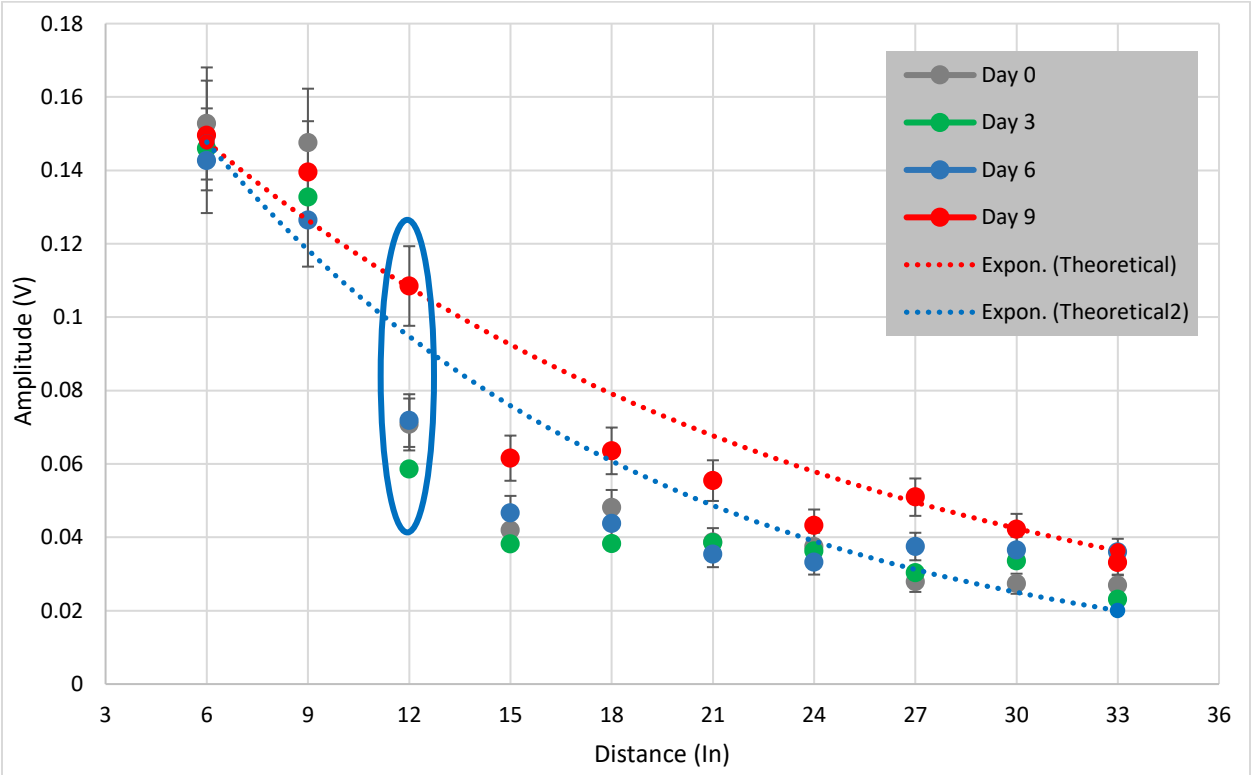

Figure 4.4 – Combined plot between Days 3, 6 and 9 versus Day 0 in 0-degree Specimen

Additionally, Figure 4.5 shows the corrosoin build-up on the naked rebar that was immersed inside the basin to visually observe corrosion progression. It can be seen that corrosion products have started to form as early as Day 6.

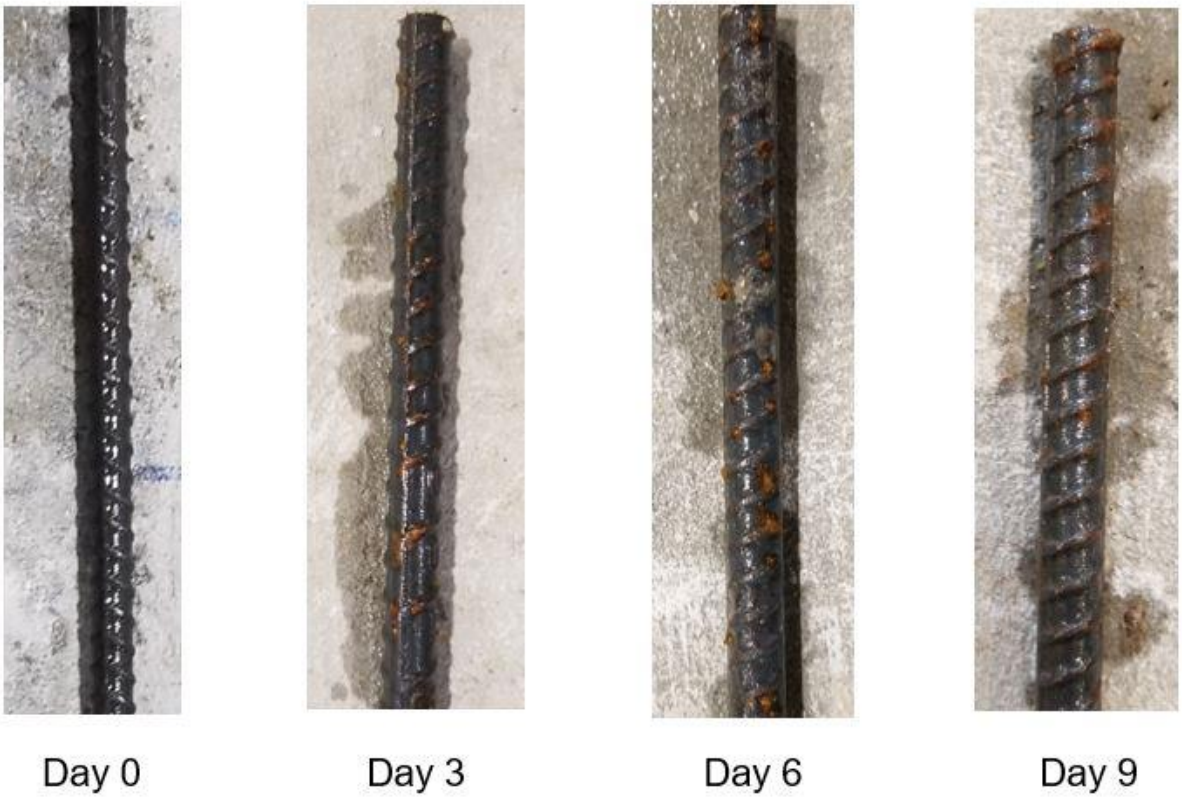

Figure 4.5 – Corrosion development on the naked bar immersed in 10% NaCl solution

To analyze the collected data from the experimental tests in this study, the change of amplitude calcualtoins were carried out by Equation 4.1 to indicate the degree of corrosoin.

$$Change\ of\ Amplitude\ (\%) = (\frac{A^i}{A^0} - 1) \times 100 \quad (4\text{-}1)$$

where:

A^i - is the amplitude of 54 kHz in the frequency domain of i^{th} increament of corrosion

A^0 - is the amplitude of 54 kHz in the frequency domain before corrosion

As shown in Figure 4.4, there is a slight increase in the measured amplitude values obtained on the Day 9 of the corrosion. Point 12-in. on Figure 4.4 shows the maximum variation in amplitude values. The change of amplitude (%) between the amplitude values for 'Day 0' and 'Day 9' for 12-in. point is about 53.5%. Figure 4.6 indicate further corrosion progression with time as there is a variation in the measured amplitude values obtained on Day 30 of corrosion. The percent channge between 'Day 0' and 'Day 30' of corrosion for Point 15 shown in Figure 4.6 is 95%.

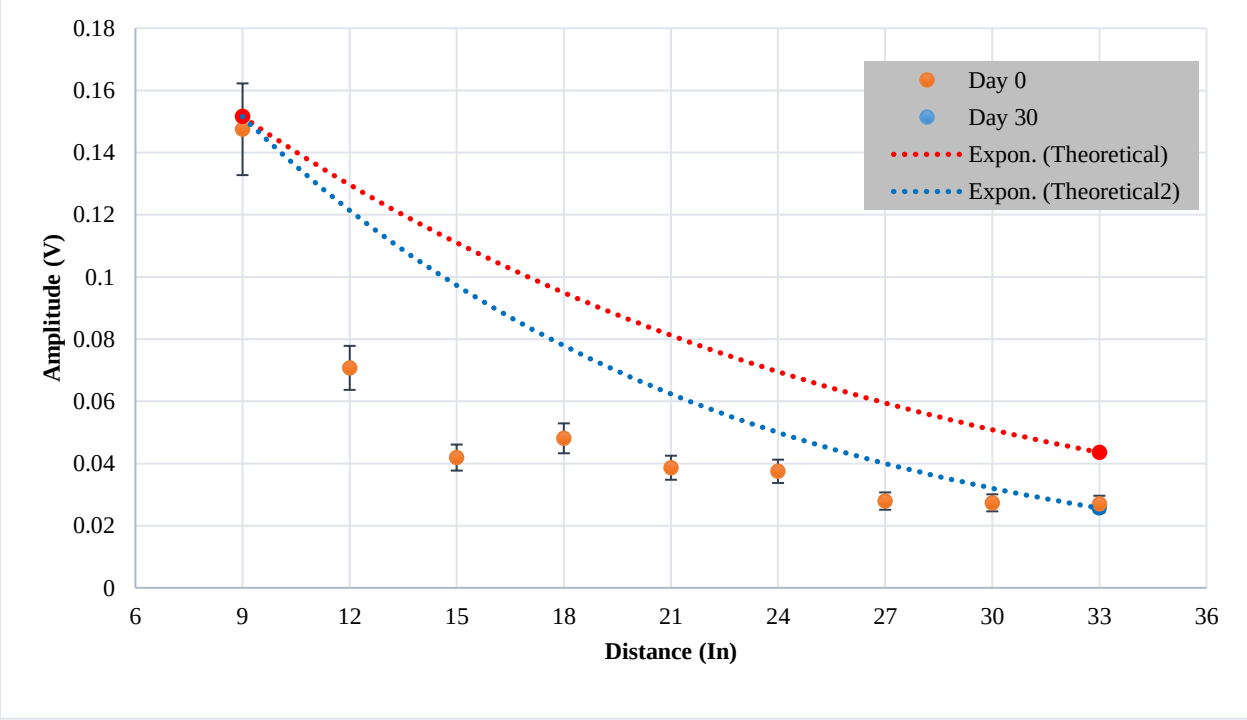

Figure 4.6 – Day 0 versus Day 30 Corrosion in 0-degree specimen

Further corrosion progression is illustratred in Figure 4.7 and Figure 4.9 for 0-degree and 33-degree specimens, respectively. In Figure 4.8, it can be observed that the corrosion has

progressed with time. Point 15-in. and Point 21-in. on Figure 4.7 represent higher variations compared to other points which indicate more corrosion progression in those points. For instance, the calculated percentage change in terms of amplitude values for Point 15-in. (shown in Figure 4.7) between 'No Corrosion' and 'Day 175' is approximately 165%.

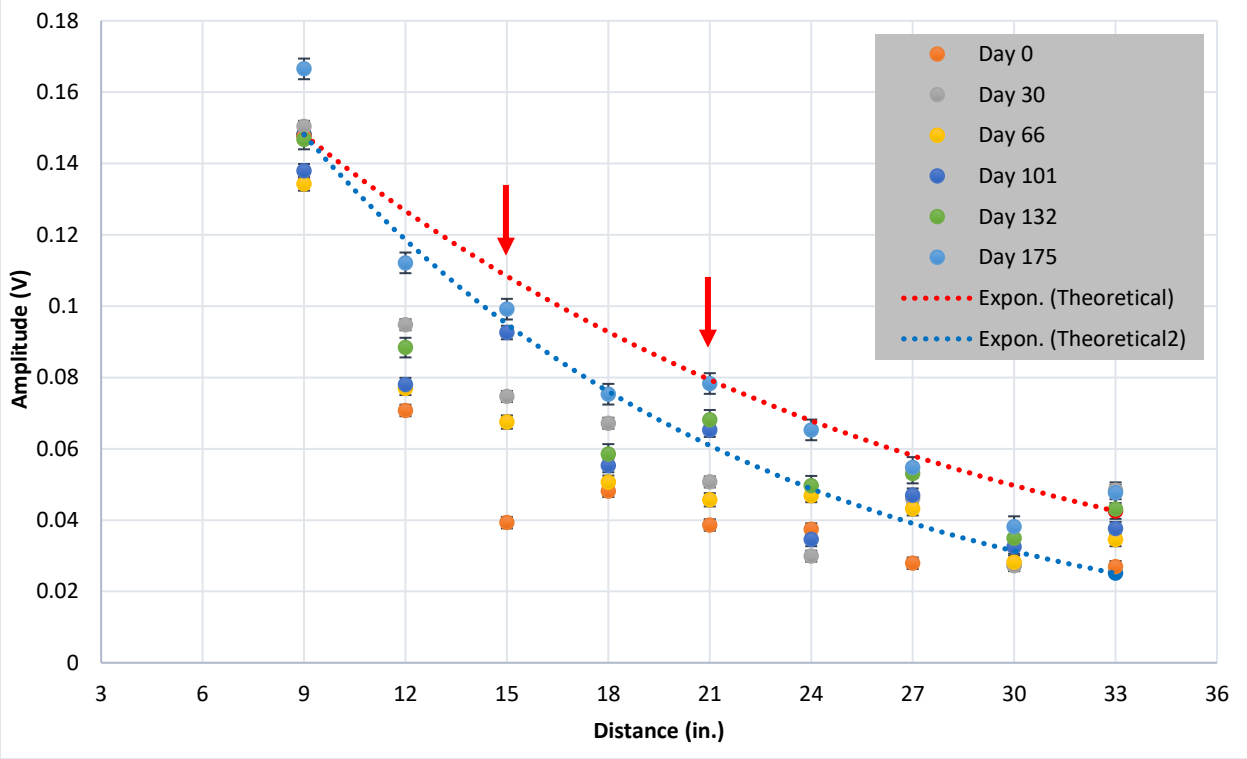

Figure 4.7 – Corrosion progression in 0-degree specimen

To further investigate the corrosion progression in these two points (Points 15-in. and 21-in. that are shown with red arrows), a daily plot is presented in Figure 4.8. An increase can be seen for both spots over the course of 175 days. However, the UGWL data has not increased in a linear form, and some data on specific days show slight decrease, which may be due to errors in testing or noise. The other reasons that may attribute to the variations in UGWL may also be related to the amount of couplant used for the test specimens.

The percent change in the amplitude values in the points 15-in. and 21-in. from 0-degree

specimen are calculated for Day 9, Day 30, Day 101, and Day 175 versus Day 0, as given in Table 4.1. The increase in the amplitude values indicate the progresssion of corrosion.

Table 4.1 – Change of amplitude for various points

UGWL Sensor Locations from Transmitter End	**Day 0**	**Day 9**		**Day 30**		**Day 101**		**Day 175**	
	Amp. (v)	Amp. (v)	**% change vs. Day 0**	Amp. (v)	**% change vs. Day 0**	Amp. (v)	**% change vs. Day 0**	Amp. (v)	**% change vs. Day 0**
15-in.	0.039	0.061	**56**	0.074	**90**	0.092	**136**	0.099	**154**
21-in.	0.038	0.055	**45**	0.051	**34**	0.065	**71**	0.078	**105**

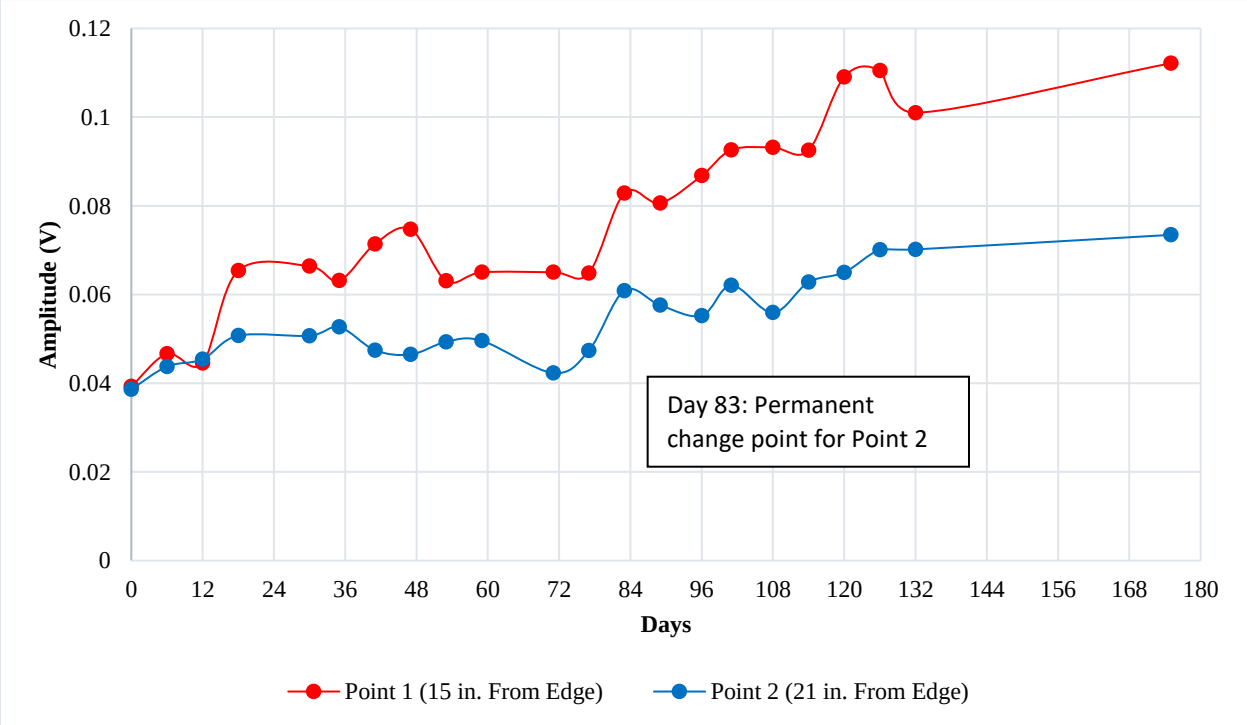

Figure 4.8 – Corrosion progression in 0-degree specimen over 175 days

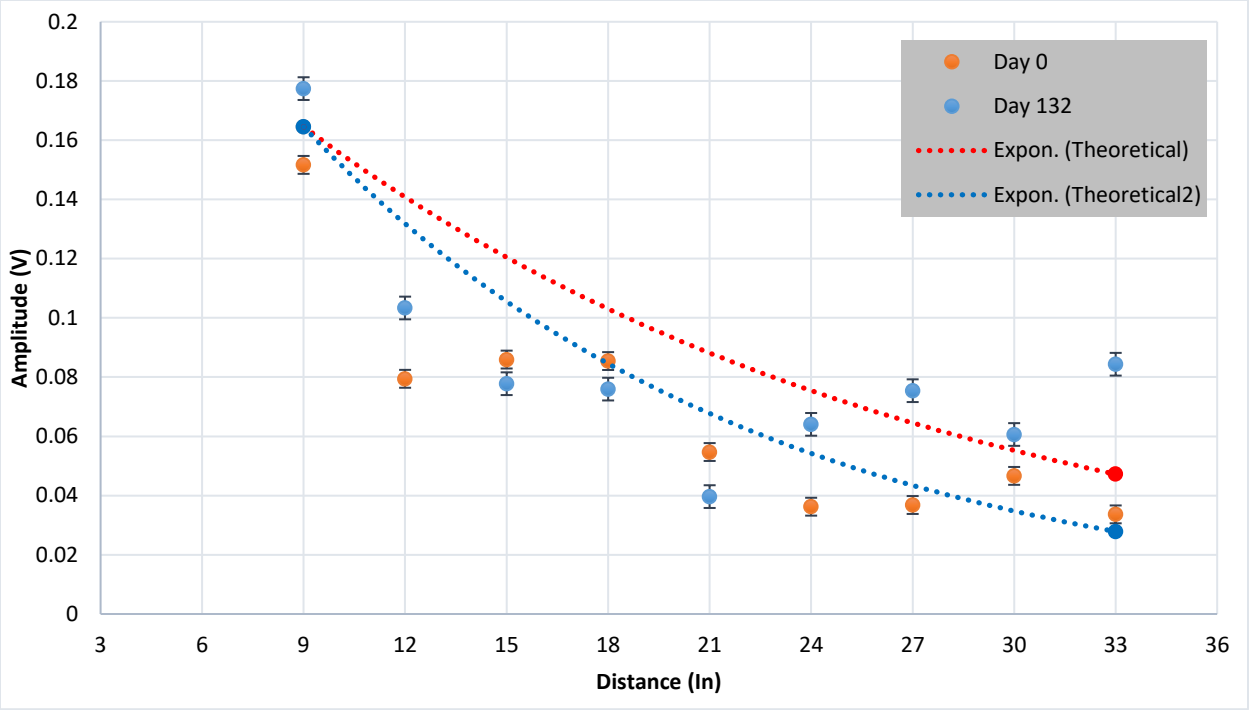

Figure 4.9 – Corrosion progression in 33-degree specimen

Figures 4.10 shows corrosion progression for 33-degree specimen. To collect UGWL data for this specimen, the signals are sent using a sensor placed on the angled end of the bar (33-degree), and received on an array of sensors on the concrete surface. Similary, a daily plot (shown in Figure 4.11) was made for two points (Points 9-in. and 27-in) in this specimen to demonstrate variations in UGWL data over time.

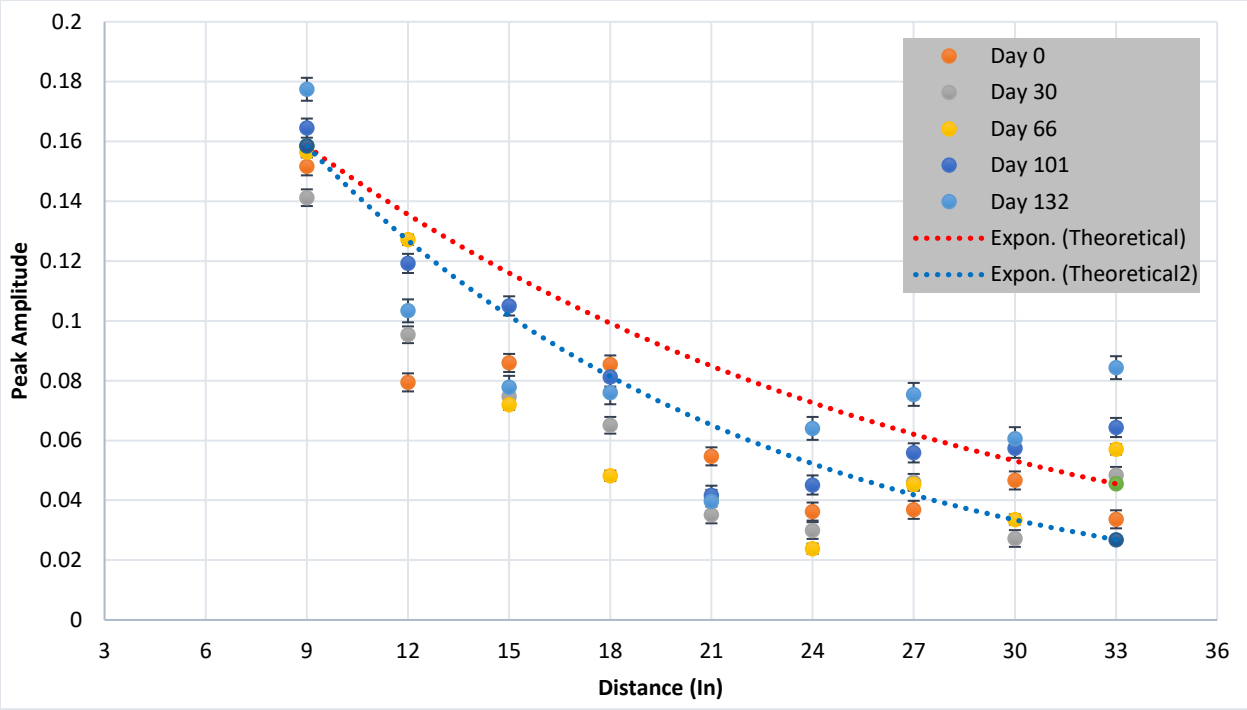

Figure 4.10 – Corrosion progression in 33-degree specimen

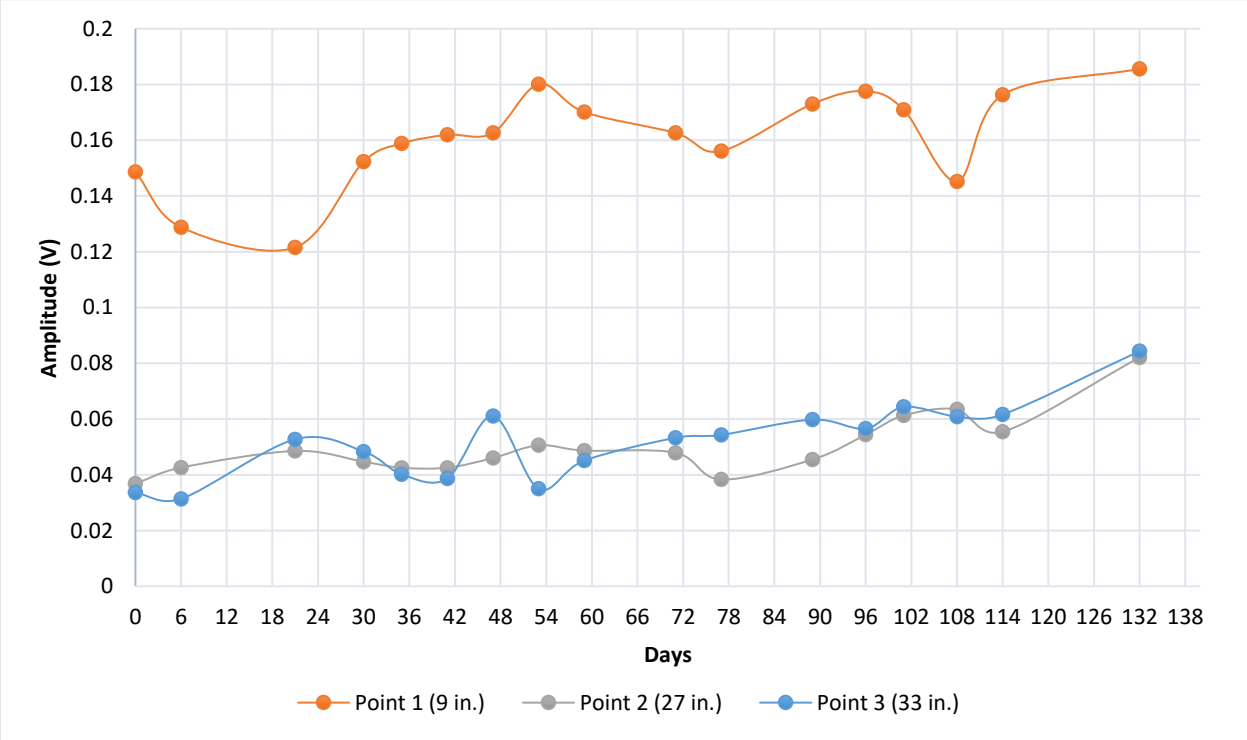

Figure 4.11 – Corrosion progression in 33-degree specimen over 132 days

Additionally, after the corrosion process was completed, an autopsy was performed on

the 33-degree specimen. Figure 12 shows the rust formation on the rebar that was embedded in 33-degree specimen.

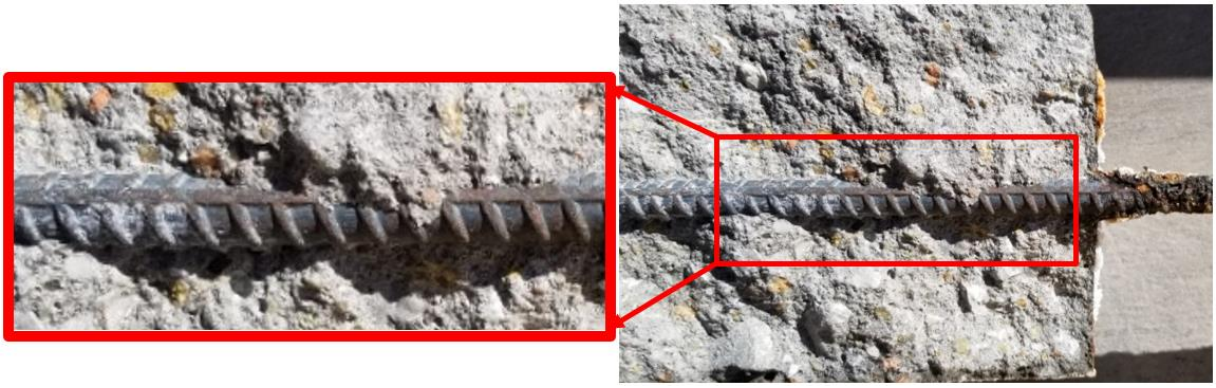

Figure 12 – Corrosion on the rebar embedded in 33-degree specimen

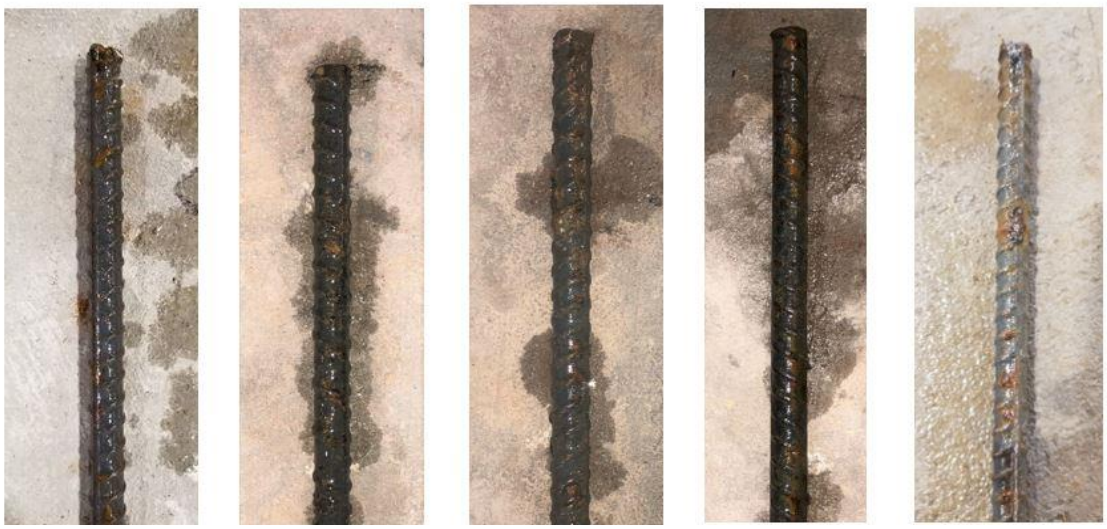

Day 30 Day 66 Day 101 Day 132 Day 175

Figure 4.13 – Corrosion development on the naked bar immersed in 10% NaCl solution

4.2 Monitoring Corrosion using Half-cell Potential

Half-cell potential tests were performed using ICOR device every 6 days on the same day as the ultrasonic measurements. Five test spots were selected and marked along the rebar on the surface of the specimen as shown in Figure 3.6 (b). The half-cell potential data obtained using

ICOR device are presented in terms of volts. ASTM C876 provides a standard based on which the probability of corrosion presence can be measured as shown in Table 2.4. The dotted lines shown in Figure 4.14 and Figure 4.15 indicate the limits specified by ASTM C876.

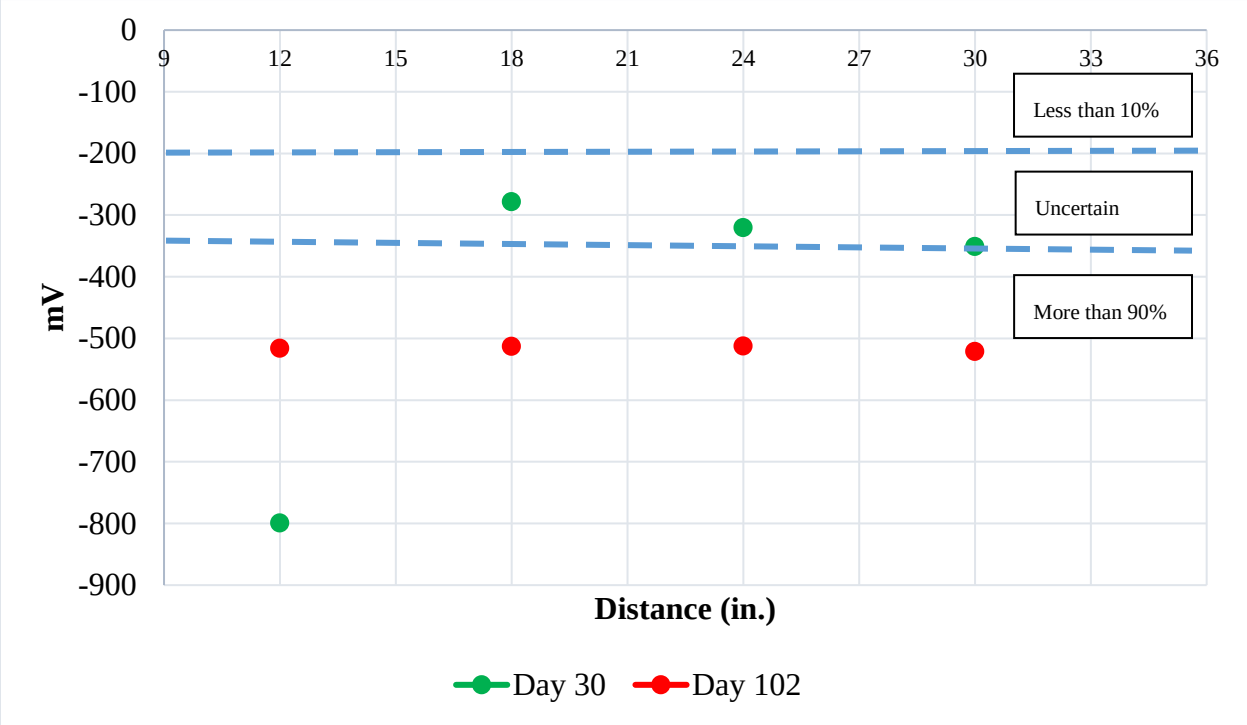

Figure 4.14 – Half-cell potential measurements for 0-degree specimen

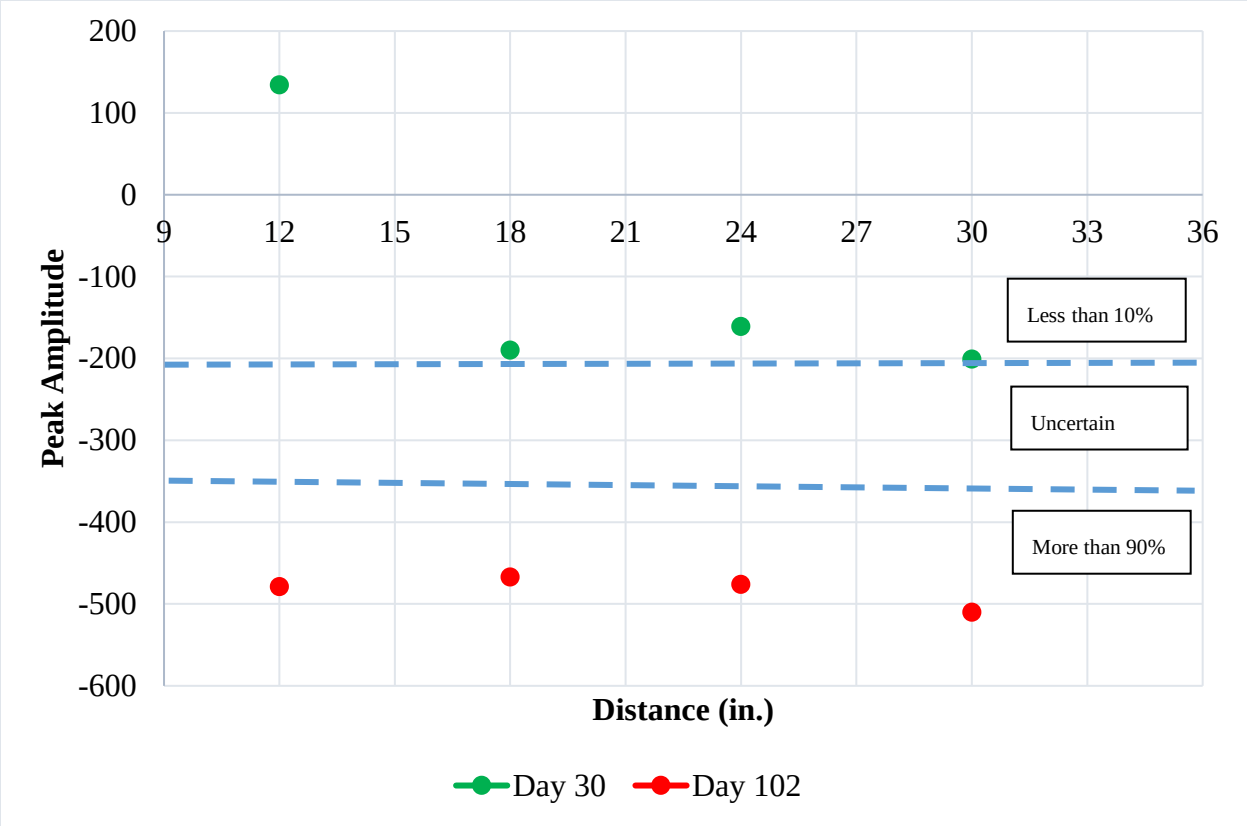

Figure 4.15 – ICOR Half-cell potential measurements for 33-degree specimen

From Figure 4.14, it can be seen that the Half-cell potential measurements for Day 30 are in the 'uncertain' range according to the interpretations given by ASTM C876, and the half-cell potential data for 33-degree show a risk of corrosion activity of less than 10%, as shown in Figure 4.14. This indicates a probability of more than 90 % for corrosio acitivity. UGWL data showed increase in the amplitute values for Day 30 for both 0-degree and 33-degree specimens. This may be stated that the corrosion was detected by UGWL method earlier than the Half-cell potential method. The earliest significant changes in the data from both methods are presented in Table 4.2.

Table 4.2 – Earliest significant change in data

Specimens	Earliest date of significant change in data	
	UGWL	HCP
0-Degree	Day 9	Day 30
33-Degree	Day 9	Day 30

4.3 Measurement of Chloride Content

The chloride content was measured accoridng to the procedure discussed in chapter 3. 0-degree specimen was selected for chloride content analysis. Since UGWL data showed the maximum variations for Points 15-in. and 21-in., these two spots were selected for this purpose and two cores were made.

The chloride content analyses were carried out using acid-soluble test according to ASTM C1152. Ion Chromatography was used to determine total chloride content per weight of concrete for the concrete samples taken from Points 15-in. and 21-in. Two iterations were done to get more reliable results. Additionally, purified water was included in the analysis to verify the validity of the results, and hypothetically, purified water should show a very small amount of chloride concentration.

The results for chloride content analysis are given in Table 4.3 and Table 4.4 for the first and second iterations. Moreover, Table 4.5 presents the average percentage of chloride concenttaions given in Tables 4.3 and 4.4..

Table 4.3 – Percentage of chlorite content per weight of concrete (1st iteration)

Sample	Mass (g)	Volume (L)	Solution (ppm)	%Cl per Concrete weight
Purified Water			0.128	
15-in.	2.1008	0.2500	70.62	0.84%
21-in.	2.1037	0.2500	47.486	0.56%
30-in.	1.9880	0.2500	15.181	0.19%

Table 4.4 – Percentage of chlorite content per weight of concrete (2nd iteration)

Sample	Mass (g)	Volume (L)	Solution (ppm)	%Cl per Concrete Weight
Purified Water			Not Detected	
15-in.	2.0425	0.2500	68.745	0.84%
21-in.	1.9692	0.2500	42.667	0.54%
30-in.	2.0100	0.2500	14.209	0.18%

The results presented in Tables 4.3 and 4.4 are more than the CTL specified by ACI 318 and Technology in Practice (TIP) that ranges between 0.05 to 0.1% by weight of concrete, which indicate a risk of corrosion activity. This can be concluded that chloride ingress has happeneed and caused the corrosion to initiate.

Table 4.5 – Percentage of chlorite content per weight of concrete

Sample	Average %Cl per Concrete Weight
15-in.	0.84%
21-in.	0.55%
31-in.	0.185%

All of the results psented in Tables 4.5 exceed the CTL specified by Technology in Practice (TIP) that ranges from 0.05 to 0.1% by weight of concrete; and all except one (31-inch point) exceed the limit. Therefore, it can be concluded that the chloride content in this specimen has exceeded the CTLs, which is an indication of corrosion activity.

Table 4.6 shows the correlation between the percentrage change in the amplitude values from UGWL measurements obtained for Points 15-in. and 21-in. in 0-degree Specimen, as well as the percernage of chloride content in concrete. There is a higher percentage change in in amplitude values in case of Point 15-in., as well as a higher chloride concentration at this point. Therefore, a good correlation is observed between UGWL data and chloride contents. In general, almost a directly proportional relationship can be seen between the UGWL measurements and chloride content. The correlation is also demonstrated in Figure 4.16.

Table 4.6 – Correlation between CTL and UGWL data

Measurement Location	UGWL Data			HCP Data		
	Day 0 (Amplitude)	Day 175 (Amplitude)	Percentage Change in UGWL reading (%)	Day 175 Reading (mV)	Day 175 Probability of Corrosion Activity	Average %Cl per Concrete Weight
15-inch	0.039	0.099	154 %	-624	>90%	0.84%
21-inch	0.038	0.078	105 %	-595	>90%	0.55%
30-inch	0.027	0.038	40 %	-574	>90%	0.185%

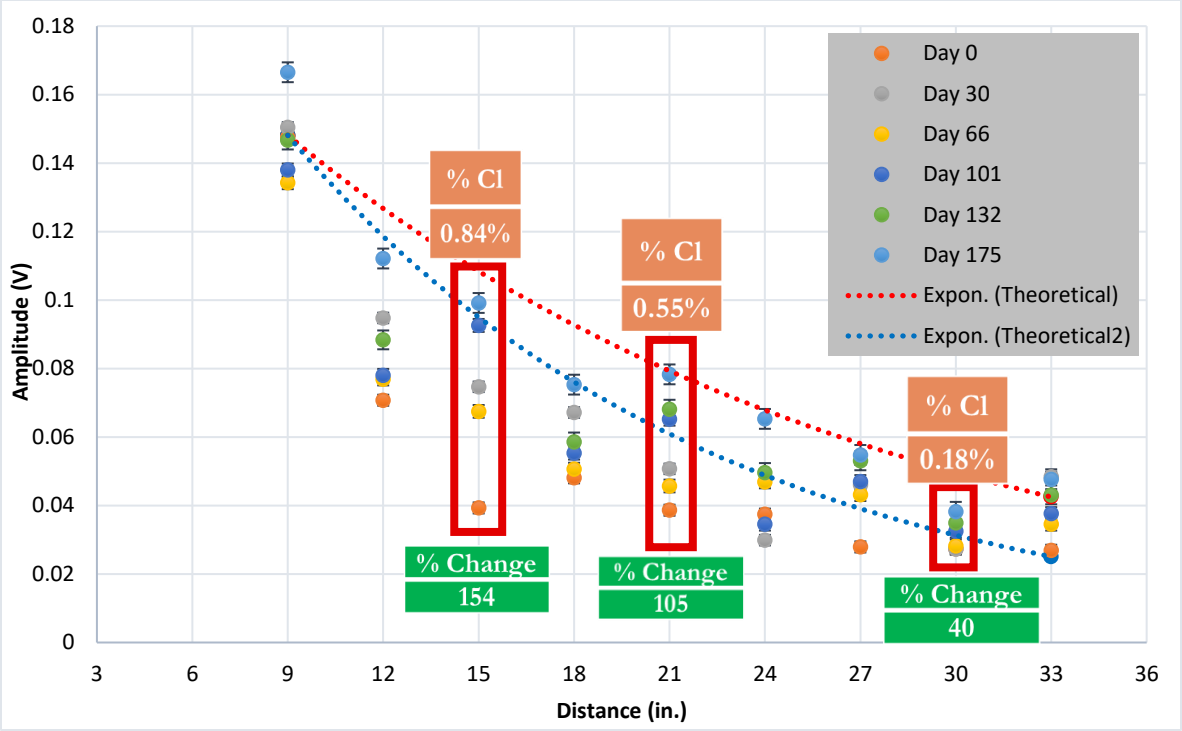

Figure 4.16 – Correlation between UGWL data and chloride content

4.4 Bar End Angles

The experimental data collect by UGWL method show the amount of energey trasmission through the wave guide (steel) with different bar end angles: 0-degree, 33-degree, and 45-degree as illustrated in Figure 3.5. The leaked energy through the concretre was monitored using the receiver on different locations on the concrete slab. Figures 4.17 shows the comparison plot obtained for these specimens. It was observed maximum energy transfer was achieved with 0- and 33-degree specimens; while in case of 45-degree specimen, less energy was transmitted. The data are presented in terms of amplitude values. In case of 45-degree specimen, since the sensor is attached to the end of the rebar at a steeper angles compared to 0-degree and 45-degree, part of the energy may be lost and not propagated through the rebar.

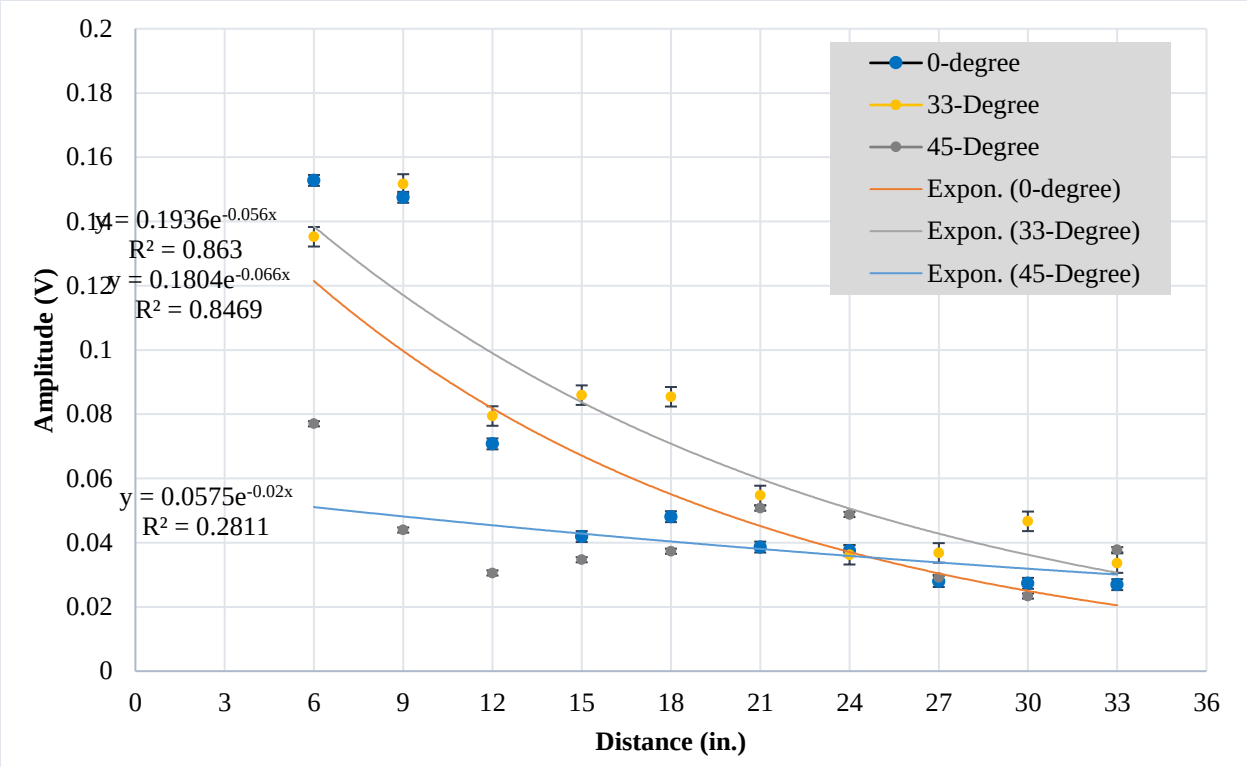

Figure 4.17 – Comparison of the UGWL data for the 0-, 33-, and 45-degree specimens

CHAPTER 5

CONCLUSIONS AND FUTURE WORK

This study provides valuble findings regarding the use of ultrasonic testing methods for corrosion monitoring, and identifies areas that need further research, which are discussed in this chapter.

5.1 Conclusions

Following conclusions are drawn from the experimental work and literature review conducted in this study:

1. The findings suggest that when UGWL and HCP are benchmarked, both methods detected the corrosion activity in laboratory specimens.
2. UGWL measurements demonstrated significant change of 90% in amplitude as early as 30 days versus Day 0 for Point 15-in. in 0-degree specimen. Similarly, 34% change between Day 0 and Day 30 was observed in the amplitue readings for Point 21-in. in 0-degree specimen after being soaked in 10% NaCl solution. Given nothing else was altered during this period this change in amplitude is attributed to corrosion activity. The sinigificant change in UGWL amplitudes compared to the uncertainty of HCP measurements on the same day of measurement suggests UGWL may detect changes in condition sooner. The experimental results also suggest that some changes in UGWL measurements started as early as 9 days for the lab specimens submerged in 10% NaCl, whereas a siginifact change in the HCP readigs were observed on Day 30 of the

corrosion. Thus, for this set of experiments UGWL method detected corrosion activity 21 days sooner than HCP.

3. From the experimental results it can be concluded that 50% change in UGWL data may be considered as the threshold for a “significant change” in the condition of reinforced concrete structures. Over a period of 175 days, the change in UGWL amplitudes were as high as 154% as compared to the baseline. The 154% increase in UGWL amplitude change correlated to a 0.84% chloride content, which is an indication that CTL has exceeded the threshold limits for chloride content such as the limits specified by ACI 318.
4. Different bar end angles (0-, 33-, and 45-degree) were used for ultrasonic measurements to find out the amount of energy transfer with each angle. It was observed that specimens having rebars with 0-degree and 33-degree bar end angles provide stronger signals then those obtained from the 45-degree bar end angle. The percent change between amplitudes observed at 6 in. in 33-degree and 45-degree bar end angles is approximately 75%. Similarly, the percent change between 0-degree and 45-degree for the same test location is almost 99%. A such, the optimal angle of attachment lies between 0- and 33-degrees from vetical. Thereofore, higher amount of energy is transferred when the transmitted when the rebar end angle is between 0- and 45-degrees.

5.2 Recommendations for Future Work

The following recommendations are made in this study for further research pertaining to use of UGWL method in identifying and monitoring the corrosion in reinforced concrete structures such as bridge decks.

1. Further research can be conducted to investigate corrosion activity in reinforced concrete structures using UGWL and HCP for a longer period of time than 6 months to observe further change in the condition of structure, to the point at which delamination may occur.
2. A more in-depth study of chloride threshold level in reinforced concrete structures may be done by establishing a profile showing concentrations of NaCl at different depths of the concrete on different days of corrosion progression.
3. To see the change in the chloride level over time, the chloride content analysis can be done at different stages throughout the research.
4. Further investigations may be made to assess the feasibility of angle beam wedges for improved attachment of the sensors on the test materials in UGWL method.
5. A method may be developed to extract small sample sizes of concrete powder non-destructively as opposed to taking cores.

REFERENCES

2002 Conditions and Performance—Policy | Federal Highway Administration. (n.d.). Retrieved May 22, 2019, from https://www.fhwa.dot.gov/policy/2002cpr/

Abbas, S., Soliman, A. M., & Nehdi, M. L. (2014). Chloride ion penetration in reinforced concrete and steel fiber-reinforced concrete precast tunnel lining segments. *Materials Journal*, *111*(6), 613–622.

ACI Committee, and International Organization for Standardization. "Building code requirements for structural concrete (ACI 318-08) and commentary." American Concrete Institute, 2008.

Ahmad, Z. (2006). *Principles of corrosion engineering and corrosion control*. Elsevier.

Aïtcin, P.-C., & Flatt, R. J. (2015). *Science and technology of concrete admixtures*. Woodhead Publishing.

Akhtar, S. (2013). Review of nondestructive testing methods for condition monitoring of concrete structures. *Journal of Construction Engineering*, *2013*.

Aktan, A. E., Farhey, D. N., Brown, D. L., Dalal, V., Helmicki, A. J., Hunt, V. J., & Shelley, S. J. (1996). Condition assessment for bridge management. *Journal of Infrastructure Systems*, *2*(3), 108–117.

Amjad, U., Yadav, S. K., & Kundu, T. (2015). Detection and quantification of diameter reduction due to corrosion in reinforcing steel bars. *Structural Health Monitoring*, *14*(5), 532–543.

Angst, U., Elsener, B., Larsen, C. K., & Vennesland, Ø. (2009). Critical chloride content in reinforced concrete—A review. *Cement and Concrete Research*, *39*(12), 1122–1138.

Ann, K. Y., & Song, H.-W. (2007). Chloride threshold level for corrosion of steel in concrete. *Corrosion Science*, *49*(11), 4113–4133.

ASTM, C. (1999). 876-99 Standard, Test method for half-cell potentials of uncoated reinforcing steel in concrete. *West Conshohocken, PA, American Society for Testing and Materials*.

ASTM, C. (2012). *Standard test method for acid-soluble chloride in mortar and concrete*.

Balakumaran, S. S. G. (2010). *Influence of Bridge Deck Concrete Parameters on the Reinforcing Steel Corrosion* [PhD Thesis]. Virginia Tech.

Balayssac, J.-P., & Garnier, V. (2017). *Non-destructive testing and evaluation of civil engineering structures*. Elsevier.

Basheer, P. A. M., Chidiact, S. E., & Long, A. E. (1996). Predictive models for deterioration of concrete structures. *Construction and Building Materials*, *10*(1), 27–37. https://doi.org/10.1016/0950-0618(95)00092-5

Bastidas-Arteaga, E., & Stewart, M. G. (2016). Economic assessment of climate adaptation strategies for existing reinforced concrete structures subjected to chloride-induced corrosion. *Structure and Infrastructure Engineering*, *12*(4), 432–449.

C09 Committee. (n.d.). *Test Method for Water-Soluble Chloride in Mortar and Concrete*. ASTM International. https://doi.org/10.1520/C1218_C1218M-17

Cho, H.-C., Ju, H., Oh, J.-Y., Lee, K. J., Hahm, K. W., & Kim, K. S. (2016). Estimation of concrete carbonation depth considering multiple influencing factors on the deterioration of durability for reinforced concrete structures. *Advances in Materials Science and Engineering*, *2016*.

Civil Engineering Materials. (2016). Elsevier. https://doi.org/10.1016/C2014-0-03170-X

Clemeña, G. G., Lane, D. S., Freeman, T. E., & Lozev, M. G. (2000). *Evaluation of nondestructive evaluation methods for application in early detection of deterioration in concrete pavements*. United States. Federal Highway Administration.

Codes, A. C. I. C. D. A. for A. B. (1985). *Guide for the design and construction of fixed offshore concrete structures*. ACI.

Cui, J. (2012). *Multiple Sensor Periodic Nondestructive Evaluation on Concrete Bridge Deck Maintenance*. University of Vermont.

Delatte, N. (2009). *Failure, distress and repair of concrete structures*. Elsevier.

Du, G., & Karoumi, R. (2013). Life cycle assessment of a railway bridge: Comparison of two superstructure designs. *Structure and Infrastructure Engineering*, *9*(11), 1149–1160.

Dunker, K. F., & Rabbat, B. G. (1990). Highway bridge type and performance patterns. *Journal of Performance of Constructed Facilities*, *4*(3), 161–173.

El Hajj, B., Schoefs, F., Castanier, B., & Yeung, T. (2017). A condition-based deterioration model for the stochastic dependency of corrosion rate and crack propagation in corroded concrete structures. *Computer-Aided Civil and Infrastructure Engineering*, *32*(1), 18–33.

Elsener, B., Andrade, C., Gulikers, J., Polder, R., & Raupach, M. (2003). Hall-cell potential measurements—Potential mapping on reinforced concrete structures. *Materials and Structures*, *36*(7), 461–471.

Erdogmus, E., Garcia, E., Amiri, A. S., & Schuller, M. (2020). A Novel Structural Health Monitoring Method for Reinforced Concrete Bridge Decks Using Ultrasonic Guided Waves. *Infrastructures*, *5*(6), 49.

Ervin, Benjamin L., Kuchma, D. A., Bernhard, J. T., & Reis, H. (2009). Monitoring corrosion of rebar embedded in mortar using high-frequency guided ultrasonic waves. *Journal of Engineering Mechanics*, *135*(1), 9–19.

Ervin, Benjamin Lee. (2007). *Monitoring corrosion of rebar embedded in mortar using guided ultrasonic waves*.

Fontana, M. G. (1986). *Corrosion Engineering*. Nace.

Frølund, T., Klinghoffer, O., Sørensen, H. E., & Denmark, D. D. (2003). Pro's and con's of half-cell potentials and corrosion rate measurements. *International Conference on ''Structural Faults*.

Garcia, E., Erdogmus, E., Schuller, M., & Harvey, D. (2017). Novel Method for the Detection of Onset of Delamination in Reinforced Concrete Bridge Decks. *Journal of Performance of Constructed Facilities*, *31*(6), 04017102.

Garcia, E. V. C. (2016). *Identifying the onset, type, and location of deterioration in reinforced concrete using ultrasonic testing*.

Garcia, Eric, Erdogmus, E., Schuller, M., & Harvey, D. (2019). Detecting Onset of Different Types of Flaws in Reinforced Concrete. *ACI Materials Journal*, *116*(1). https://doi.org/10.14359/51710962

Gazis, D. C. (1959). Three-Dimensional Investigation of the Propagation of Waves in Hollow Circular Cylinders. II. Numerical Results. *The Journal of the Acoustical Society of America*, *31*(5), 573–578.

Glass, G. K., & Buenfeld, N. R. (2000). Chloride-induced corrosion of steel in concrete. *Progress in Structural Engineering and Materials*, *2*(4), 448–458.

Glass, G. K., Reddy, B., & Buenfeld, N. R. (2000). Corrosion inhibition in concrete arising from its acid neutralisation capacity. *Corrosion Science*, *42*(9), 1587–1598.

Goodway, B. (2001). AVO and Lamé constants for rock parameterization and fluid detection. *CSEG Recorder*, *26*(6), 39–60.

Gucunski, N., & Council, N. R. (2013). *Nondestructive testing to identify concrete bridge deck deterioration*. Transportation Research Board.

Haldar, S. K. (2018). Chapter 6—Exploration Geophysics. In S. K. Haldar (Ed.), *Mineral Exploration (Second Edition)* (pp. 103–122). Elsevier. https://doi.org/10.1016/B978-0-12-814022-2.00006-X

Hartt, W. H., Powers, R. G., Leroux, V., & Lysogorski, D. K. (2004). *A CRITICAL LITERATURE REVIEW OF HIGH-PERFORMANCE CORROSION REINFORCEMENTS IN CONCRETE BRIDGE APPLICATIONS*. https://trid.trb.org/view/703200

Hausmann, D. A. (1967). Steel corrosion in concrete–How does it occur? *Materials Protection*.

Helal, J., Sofi, M., & Mendis, P. (2015). Non-destructive testing of concrete: A review of methods. *Electronic Journal of Structural Engineering*, *14*(1), 97–105.

Hema, J., & Guthrie, W. S. (n.d.). *CONCRETE BRIDGE DECK CONDITION ASSESSMENT AND IMPROVEMENT STRATEGIES*. 151.

Ji, Y., Zhao, W., Zhou, M., Ma, H., & Zeng, P. (2013). Corrosion current distribution of macrocell and microcell of steel bar in concrete exposed to chloride environments. *Construction and Building Materials*, *47*, 104–110.

John, D. G., Searson, P. C., & Dawson, J. L. (1981). Use of AC impedance technique in studies on steel in concrete in immersed conditions. *British Corrosion Journal*, *16*(2), 102–106.

Karakurt, C., & Topçu, İ. B. (2012). Effect of blended cements with natural zeolite and industrial by-products on rebar corrosion and high temperature resistance of concrete. *Construction and Building Materials*, *35*, 906–911.

Kelly, T. D. (1998). *Crushed cement concrete substitution for construction aggregates, a materials flow analysis*. US Department of the Interior, US Geological Survey.

Kendall, A., Keoleian, G. A., & Helfand, G. E. (2008). Integrated life-cycle assessment and life-cycle cost analysis model for concrete bridge deck applications. *Journal of Infrastructure Systems*, *14*(3), 214–222.

Li, D., Ruan, T., & Yuan, J. (2012). Inspection of reinforced concrete interface delamination using ultrasonic guided wave non-destructive test technique. *Science China Technological Sciences*, *55*(10), 2893–2901.

Liu, R., Jiang, L., Xu, J., Xiong, C., & Song, Z. (2014). Influence of carbonation on chloride-induced reinforcement corrosion in simulated concrete pore solutions. *Construction and Building Materials*, *56*, 16–20. https://doi.org/10.1016/j.conbuildmat.2014.01.030

Lounis, Z., & Vanier, D. J. (1998). *Optimization of bridge maintenance management using Markovian models*.

Manning, D. G. (1985). Detecting defects and deterioration in highway structures. *NCHRP Synthesis of Highway Practice*, *118*.

Marine Concrete Structures. (2016). Elsevier. https://doi.org/10.1016/C2014-0-01042-8

Meck, E., & Sirivivatnanon, V. (2003). Field indicator of chloride penetration depth. *Cement and Concrete Research*, *33*(8), 1113–1117. https://doi.org/10.1016/S0008-8846(03)00012-7

Miller, T. H. (2010). *Nondestructive inspection of corrosion and delamination at the concrete-steel reinforcement interface*.

Mustapha, S., Lu, Y., Li, J., & Ye, L. (2014). Damage detection in rebar-reinforced concrete beams based on time reversal of guided waves. *Structural Health Monitoring*, *13*(4), 347–358.

NRMCA | TiPs: Technology in Practice. (n.d.). Retrieved February 9, 2020, from https://www.nrmca.org/aboutconcrete/tips/default.asp

Oh, B. H., Jang, S. Y., & Shin, Y. S. (2003). Experimental investigation of the threshold chloride concentration for corrosion initiation in reinforced concrete structures. *Magazine of Concrete Research*, *55*(2), 117–124.

Page, C. L., & Havdahl, J. (1985). Electrochemical monitoring of corrosion of steel in microsilica cement pastes. *Materials and Structures*, *18*(1), 41–47.

Pradhan, B., & Bhattacharjee, B. (2009). Half-cell potential as an indicator of chloride-induced rebar corrosion initiation in RC. *Journal of Materials in Civil Engineering*, *21*(10), 543–552.

Pradhan, B., & Bhattacharjee, B. (2011). Rebar corrosion in chloride environment. *Construction and Building Materials*, *25*(5), 2565–2575.

Rahman, M. K., Al-Kutti, W. A., Shazali, M. A., & Baluch, M. H. (2012). Simulation of chloride migration in compression-induced damage in concrete. *Journal of Materials in Civil Engineering*, *24*(7), 789–796.

Rakotovao Ravahatra, N., Bastidas-Arteaga, E., Schoefs, F., De Larrard, T., & Duprat, F. (2019). Probabilistic and sensitivity analysis of analytical models of corrosion onset for reinforced concrete structures. *European Journal of Environmental and Civil Engineering*, 1–30.

Rose, J.L. (1999) Ultrasonic Waves in Solid Media. Cambridge University Press, Cambridge. - References—Scientific Research Publishing. (n.d.). Retrieved May 21, 2019, from https://www.scirp.org/(S(vtj3fa45qm1ean45vvffcz55))/reference/ReferencesPapers.aspx?ReferenceID=1896876

Schiessl, P., & Lay, S. (2005). Influence of concrete composition. *Corrosion in Reinforced Concrete Structures*, 91–134.

Scott, M., Rezaizadeh, A., Delahaza, A., Santos, C. G., Moore, M., Graybeal, B., & Washer, G. (2003). A comparison of nondestructive evaluation methods for bridge deck assessment. *NDT & E International*, *36*(4), 245–255. https://doi.org/10.1016/S0963-8695(02)00061-0

Sriramadasu, R. C., Banerjee, S., & Lu, Y. (2019). Detection and assessment of pitting corrosion in rebars using scattering of ultrasonic guided waves. *NDT & E International*, *101*, 53–61.

Standard, B. (1997). *Structural Use of Concrete: Code of Practice for Design and Construction, Part 1, BS 8110*. British Standard Institution, UK.

Stratfull, R. F. (1957). The corrosion of steel in a reinforced concrete bridge. *Corrosion*, *13*(3), 43–48.

Structural Health Monitoring with Piezoelectric Wafer Active Sensors. (2014). Elsevier. https://doi.org/10.1016/C2013-0-00155-7

Sun, Z., Zhang, L., & Rose, J. L. (2005). Flexural torsional guided wave mechanics and focusing in pipe. *Journal of Pressure Vessel Technology*, *127*(4), 471–478.

Tesfamariam, S., Bastidas-Arteaga, E., & Lounis, Z. (2018). Seismic Retrofit Screening of Existing Highway Bridges With Consideration of Chloride-Induced Deterioration: A Bayesian Belief Network Model. *Frontiers in Built Environment*, *4*.

Types and causes of concrete deterioration. (2002). Portland Cement Association.

Wang, M. L., Lynch, J. P., & Sohn, H. (2014). *Sensor Technologies for Civil Infrastructures, Volume 1: Sensing Hardware and Data Collection Methods for Performance Assessment*. Elsevier.

Waqar, S., Wang, L., & John, S. (2015). Piezoelectric energy harvesting from intelligent textiles. In *Electronic Textiles* (pp. 173–197). Elsevier.

Wheat, H. G., & Eliezer, Z. (1985). Some electrochemical aspects of corrosion of steel in concrete. *Corrosion*, *41*(11), 640–645.

Yuan, Y., Ji, Y., & Jiang, J. (2009). Effect of corrosion layer of steel bar in concrete on time-variant corrosion rate. *Materials and Structures*, *42*(10), 1443–1450. https://doi.org/10.1617/s11527-008-9464-9

Zemajtis, J. (1998). *Modeling the time to corrosion initiation for concretes with mineral admixtures and/or corrosion inhibitors in chloride-laden environments* [PhD Thesis]. Virginia Tech.

Zivica, V. (2003). Corrosion of reinforcement induced by environment containing chloride and carbon dioxide. *Bulletin of Materials Science*, *26*(6), 605–608. https://doi.org/10.1007/BF02704323

APPENDIX A: UGWL MEASUREMENTS

	Specimen: Corrosion 0 deg.			
Corrosion				
Baseline				
File name	Distance (in.)	Amplitude	Avg.	Standard Deviation
1	6	0.150251495	0.152782	0.00247652
2	6	0.14978043		
3	6	0.149684503		
4	6	0.153090621		
5	6	0.153067651		
6	6	0.152446999		
7	6	0.152464778		
8	6	0.150888786		
9	6	0.150600732		
10	6	0.150693112		
11	6	0.154090369		
12	6	0.156420404		
13	6	0.156242826		
14	6	0.155808281		
15	6	0.156199008		
16	9	0.149406926	0.147516767	0.000723595
17	9	0.147169112		
18	9	0.146715899		
19	9	0.146985725		
20	9	0.147603718		
21	9	0.147146226		
22	9	0.14746476		
23	9	0.147292925		

24	9	0.148130386		
25	9	0.147314775		
26	9	0.147453988		
27	12	0.069990129	0.070754544	0.001893032
28	12	0.071335243		
29	12	0.070141836		
30	12	0.074057257		
31	12	0.072398696		
32	12	0.071567359		
33	12	0.069773255		
34	12	0.07231102		
35	12	0.070992077		
36	12	0.068134882		
37	12	0.067598227		
38	15	0.038134008	0.041901834	
39	15	0.038745147		
40	15	0.047027947		
41	15	0.048332792		
42	15	0.051158129		
43	15	0.039454062		
44	15	0.039704806		
45	15	0.039476663		
46	15	0.039569723		
47	15	0.039587378		
48	15	0.039729521		
49	18	0.048866895	0.0480933	0.001048756
50	18	0.048691924		
51	18	0.047299792		
52	18	0.046896394		
53	18	0.049801898		
54	18	0.049347631		
55	18	0.048428425		
56	18	0.046680654		
57	18	0.047503041		
58	18	0.048387981		
59	18	0.047121664		
60	21	0.036674007	0.038638751	0.003058434
61	21	0.035746077		
62	21	0.037143763		
63	21	0.033614486		
64	21	0.037383698		

65	21	0.042521844		
66	21	0.044276217		
67	21	0.04006873		
68	21	0.040234708		
69	21	0.038047327		
70	21	0.039315401		
71	24	0.03842922		
72	24	0.042066722		
73	24	0.039450769		
74	24	0.040612709		
75	24	0.032635121		
76	24	0.030527372	0.037487606	0.003476522
77	24	0.039193074		
78	24	0.03786605		
79	24	0.038334494		
80	24	0.038640866		
81	24	0.034607273		
82	27	0.027485342		
83	27	0.02855644		
84	27	0.028931682		
85	27	0.027848551		
86	27	0.028675082		
87	27	0.027991971	0.027908898	0.000605894
88	27	0.028187279		
89	27	0.027355671		
90	27	0.027409426		
91	27	0.027287144		
92	27	0.027269295		
93	30	0.02965957		
94	30	0.0251097		
95	30	0.025663381		
96	30	0.027103114		
97	30	0.026445029		
98	30	0.028155078	0.027344698	0.001263333
99	30	0.027858527		
100	30	0.027361524		
101	30	0.027519201		
102	30	0.027636381		
103	30	0.028280168		
104	33	0.026255501	0.026935185	0.000820361
105	33	0.027037074		

106	33	0.026620317		
107	33	0.027181356		
108	33	0.028235954		
109	33	0.026259251		
110	33	0.025877963		
111	33	0.02643618		
112	33	0.028286198		
113	33	0.02765329		
114	33	0.026443955		

	Specimen: Corrosion 0 deg.			
Corrosion				
Day 3				
File name	Distance (in.)	Amplitude	Avg.	Standard Deviation
10	6	0.135491957	0.14595664	0.004367243
11	6	0.14237859		
12	6	0.143324352		
13	6	0.146296646		
14	6	0.148141343		
15	6	0.148562983		
16	6	0.148011531		
17	6	0.151952289		
18	6	0.146370024		
19	6	0.14564678		
20	6	0.148174955		
21	6	0.149521865		
22	6	0.149604165		
23	6	0.150176237		
24	6	0.139532108		
25	6	0.142120417		
26	9	0.127901331	0.132698976	0.007519017
27	9	0.128786271		
28	9	0.136006566		
29	9	0.129280687		
30	9	0.140064513		
31	9	0.14244658		
32	9	0.148333271		

33	9	0.125779063		
34	9	0.139580991		
35	9	0.129290112		
36	9	0.122872762		
37	9	0.124081552		
38	9	0.134461398		
39	9	0.139083562		
40	9	0.124446251		
41	9	0.130768711		
42	12	0.061283946		
43	12	0.06087224		
44	12	0.052972038		
45	12	0.054915834		
46	12	0.059694756		
47	12	0.057628406		
48	12	0.063187922		
49	12	0.056482114		
50	12	0.052431107		
51	12	0.050550726		
52	12	0.059363628	0.058532847	0.004898545
53	12	0.057146855		
54	12	0.065945998		
55	12	0.067324787		
56	12	0.065528536		
57	12	0.058706708		
58	12	0.058800473		
59	12	0.064671639		
60	12	0.053537221		
61	12	0.052130533		
62	12	0.056014314		
65	15	0.034776813		
66	15	0.032166486		
67	15	0.032785712		
68	15	0.035178387		
69	15	0.037713924		
70	15	0.033616837	0.038184123	0.003654537
71	15	0.046868954		
72	15	0.043886494		
73	15	0.042741376		
74	15	0.041395189		
75	15	0.039414139		

76	15	0.039197702		
77	15	0.038853272		
78	15	0.038210318		
79	15	0.036811249		
80	15	0.037816846		
81	15	0.037904081		
82	15	0.037471132		
83	15	0.037454089		
84	15	0.039419455		
85	18	0.036754462		
86	18	0.042392654		
87	18	0.037562344		
88	18	0.039934769		
89	18	0.035163206		
90	18	0.035363995		
91	18	0.037656466		
92	18	0.03608357	0.038253981	0.003479818
93	18	0.040789048		
94	18	0.038184397		
95	18	0.039647211		
96	18	0.033894462		
97	18	0.032579162		
98	18	0.043405357		
99	18	0.044398616		
100	21	0.029769452		
101	21	0.035548121		
102	21	0.040809106		
103	21	0.042299633		
104	21	0.045100678		
105	21	0.04129335		
106	21	0.042639803		
107	21	0.041951249	0.038502357	0.004132418
108	21	0.042921311		
109	21	0.036037268		
110	21	0.036036739		
111	21	0.036854731		
112	21	0.037957923		
113	21	0.036941015		
114	21	0.037006165		
115	21	0.032871168		
116	24	0.039871438	0.036245861	0.001600017

117	24	0.036788284		
118	24	0.037770284		
119	24	0.035146868		
120	24	0.036376801		
121	24	0.037581077		
122	24	0.037003346		
123	24	0.036053122		
124	24	0.034629845		
125	24	0.035985059		
126	24	0.033951687		
127	24	0.035459011		
128	24	0.034579367		
129	27	0.030780484	0.0302706	0.001870957
130	27	0.030830074		
131	27	0.028835824		
132	27	0.029678358		
133	27	0.02976548		
134	27	0.030536607		
135	27	0.033456353		
136	27	0.031052644		
137	27	0.033289454		
138	27	0.030936163		
139	27	0.029848348		
140	27	0.027218736		
141	27	0.027289278		
142	30	0.035106922	0.033498888	0.002386137
143	30	0.034657405		
144	30	0.031330455		
145	30	0.029249039		
146	30	0.033765624		
147	30	0.029031672		
148	30	0.033645801		
149	30	0.035158181		
150	30	0.034722393		
151	30	0.033750233		
152	30	0.036535808		
153	30	0.035033123		
154	33	0.022235069	0.023033909	0.002214988
155	33	0.026696018		
156	33	0.026447233		
157	33	0.025836704		

158	33	0.022995687		
159	33	0.02361234		
160	33	0.022965353		
161	33	0.020383647		
162	33	0.020519823		
163	33	0.021251928		
164	33	0.022013756		
165	33	0.02144935		

Corrosion				
Day 6				
File name	Distance (in.)	Amplitude	Avg.	Standard Deviation
1	6	0.141387925	0.142633672	0.001077022
2	6	0.144745156		
3	6	0.142979708		
4	6	0.141068075		
5	6	0.141231944		
6	6	0.143672744		
7	6	0.143389084		
8	6	0.143137806		
9	6	0.142726143		
10	6	0.142753656		
11	6	0.142278212		
12	6	0.142233606		
13	9	0.144211676	0.126413768	0.007156575
14	9	0.143301713		
15	9	0.119052159		
16	9	0.122305281		
17	9	0.119779641		
18	9	0.119111053		
19	9	0.119059085		
20	9	0.125833013		
21	9	0.125558813		
22	9	0.125308913		
23	9	0.125031311		

24	9	0.124900462		
25	9	0.124868369		
26	9	0.124562045		
27	9	0.124000169		
28	9	0.135256772		
29	9	0.127274384		
30	9	0.126597319		
31	9	0.125849405		
32	12	0.071224237	0.071810783	0.00491819
33	12	0.069183629		
34	12	0.066102604		
35	12	0.06556735		
36	12	0.064424497		
37	12	0.063177647		
38	12	0.077620486		
39	12	0.077185361		
40	12	0.076229856		
41	12	0.076020656		
42	12	0.07552299		
43	12	0.074633247		
44	12	0.072604769		
45	12	0.073639244		
46	12	0.073275201		
47	12	0.072560759		
48	15	0.048272516	0.046624034	
49	15	0.044798801		
50	15	0.047247767		0.002880982
51	15	0.04455158		
52	15	0.046729114		
53	15	0.046139828		
54	15	0.045669154		
55	15	0.045830247		
56	15	0.052256054		
57	15	0.052244341		
58	15	0.047970875		
59	15	0.046405313		
60	15	0.048336726		
61	15	0.047766051		
62	15	0.048122013		
63	15	0.046792821		
64	15	0.048079478		

65	15	0.047963158		
66	15	0.04793356		
67	15	0.047828399		
68	15	0.047752148		
69	15	0.041838247		
70	15	0.041806482		
71	15	0.041925079		
72	15	0.041341088		
73	18	0.039926784	0.043769244	0.004683949
74	18	0.039291825		
75	18	0.038814152		
76	18	0.038553248		
77	18	0.038150183		
78	18	0.048759995		
79	18	0.048226506		
80	18	0.038075128		
81	18	0.049244118		
82	18	0.044499204		
83	18	0.044728284		
84	18	0.048660809		
85	18	0.048098353		
86	18	0.047740834		
87	21	0.03743913	0.035405032	0.001538849
88	21	0.037248666		
89	21	0.037038172		
90	21	0.032395188		
91	21	0.035666647		
92	21	0.035681316		
93	21	0.034939073		
94	21	0.035503726		
95	21	0.035561728		
96	21	0.034095039		
97	21	0.033886664		
98	24	0.032034	0.033159806	0.001289022
99	24	0.03184489		
100	24	0.031337333		
101	24	0.031128304		
102	24	0.033763992		
103	24	0.034498835		
104	24	0.034319122		
105	24	0.034161074		

106	24	0.034077807		
107	24	0.033878274		
108	24	0.03371424		
109	27	0.033901678		
110	27	0.039252335		
111	27	0.039142527		
112	27	0.0387713		
113	27	0.038235231		
114	27	0.038007007	0.037489268	0.001553511
115	27	0.037796315		
116	27	0.037330617		
117	27	0.037160384		
118	27	0.036791638		
119	27	0.035992916		
120	30	0.037655957		
121	30	0.037367475		
122	30	0.037083053		
123	30	0.036955151		
124	30	0.036786232		
125	30	0.036572455	0.036492398	0.00061299
126	30	0.036205432		
127	30	0.03600671		
128	30	0.035784904		
129	30	0.035603454		
130	30	0.035395554		
131	33	0.037518912		
132	33	0.036654879		
133	33	0.036443214		
134	33	0.036228704		
135	33	0.035932914		
136	33	0.03580316	0.035997744	0.000673666
137	33	0.035722954		
138	33	0.035596026		
139	33	0.035487982		
140	33	0.035360947		
141	33	0.035225489		

	Specimen: Corrosion 0 deg.	
Corrosion		
Day 9		

File name	Distance (in.)	Amplitude	Avg.	Standard Deviation
1	6	0.1462548	0.149514346	0.002609102
2	6	0.1464485		
3	6	0.1474424		
4	6	0.1509512		
5	6	0.1518548		
6	6	0.1511649		
7	6	0.1459721		
8	6	0.1517087		
9	6	0.1516812		
10	6	0.151665		
13	9	0.1379893	0.139462155	0.003267514
14	9	0.1375586		
15	9	0.1365241		
16	9	0.1360837		
17	9	0.1367931		
18	9	0.1363775		
19	9	0.1437575		
20	9	0.145		
21	9	0.143		
22	9	0.141		
23	9	0.14		
32	12	0.1118257	0.108491695	0.004708095
33	12	0.1113249		
34	12	0.1052929		
35	12	0.1161572		
36	12	0.1073948		
37	12	0.1060115		
38	12	0.113149		
39	12	0.1091568		
40	12	0.1042704		
41	12	0.1033022		
48	15	0.0613771	0.061567607	0.002882071
49	15	0.0589911		
50	15	0.0649717		
51	15	0.0631533		
52	15	0.0636844		
53	15	0.0624252		
54	15	0.0598086		
55	15	0.0555312		
56	15	0.0637445		

57	15	0.0606294		
58	15	0.0601601		
73	18	0.067199	0.063559656	0.003256998
74	18	0.0627231		
75	18	0.0656457		
76	18	0.0654463		
77	18	0.067635		
78	18	0.0636361		
79	18	0.0659026		
80	18	0.0623169		
81	18	0.0567479		
82	18	0.0604157		
83	18	0.0614878		
87	21	0.0548594	0.055449971	0.002247003
88	21	0.0538689		
89	21	0.0578265		
90	21	0.0562635		
91	21	0.0590431		
92	21	0.0543565		
93	21	0.0520399		
94	21	0.0578948		
95	21	0.0523854		
96	21	0.0554861		
97	21	0.0559256		
98	24	0.0461359	0.043251501	0.001280465
99	24	0.044994		
100	24	0.0439075		
101	24	0.0425514		
102	24	0.0428431		
103	24	0.0422671		
104	24	0.0429549		
105	24	0.0429181		
106	24	0.0429782		
107	24	0.0423264		
108	24	0.0418899		
109	27	0.0537193	0.050943578	0.001355112
110	27	0.048665		
111	27	0.0496109		
112	27	0.0494887		
113	27	0.0513406		
114	27	0.050898		

115	27	0.051647		
116	27	0.0516343		
117	27	0.0518381		
118	27	0.0517261		
119	27	0.05164		
120	27	0.0521822		
121	27	0.0524693		
122	27	0.0504729		
123	27	0.0515315		
124	27	0.0484299		
125	27	0.0512711		
126	27	0.0512632		
127	27	0.0497102		
128	27	0.0493333		
129	30	0.0415943		
130	30	0.0420374		
131	30	0.0409063		
132	30	0.0402332		
133	30	0.0405049		
134	30	0.0433936		0.001405709
135	30	0.043739	0.042173574	
136	30	0.0440645		
137	30	0.042269		
138	30	0.0424746		
139	30	0.041977		
140	33	0.0337592		
141	33	0.0287133		
142	33	0.0322806		
143	33	0.0339445		
144	33	0.0319867		
145	33	0.0302653		
146	33	0.0338158		
147	33	0.0299482	0.033140272	0.00289431
148	33	0.0310178		
149	33	0.0303747		
150	33	0.0304669		
151	33	0.0369099		
152	33	0.0369709		
153	33	0.0365539		
154	33	0.0365301		
155	33	0.0367065		

	Specimen: Corrosion 0 deg.			
Corrosion				
Day 30				
File name	Distance (in.)	Amplitude	Avg.	Standard Deviation
1	9	0.149528903	0.150427285	0.001433856
2	9	0.149136852		
3	9	0.148896135		
4	9	0.152310975		
5	9	0.151683608		
6	9	0.151007237		
7	12	0.096250092	0.094785525	0.002047222
8	12	0.095550813		
9	12	0.096919853		
10	12	0.094149955		
11	12	0.09507235		
12	12	0.094267489		
13	12	0.096491907		
14	12	0.095200269		
15	12	0.09623313		
16	12	0.093337921		
17	15	0.074725763	0.074667792	0.000678115
18	15	0.074688041		
19	15	0.075483172		
20	15	0.075671486		
21	15	0.07415704		
22	15	0.074486913		
23	15	0.074871704		
24	15	0.074649849		
25	15	0.074428593		
26	15	0.073593579		
27	18	0.064233128	0.067169366	
28	18	0.066504016		
29	18	0.066432182		
30	18	0.06655954		
31	18	0.066835837		
32	18	0.068642605		
33	18	0.067258192		
34	18	0.068421715		

35	18	0.069637081		
36	21	0.035443079	0.035098723	0.000395379
37	21	0.034969048		
38	21	0.035155169		
39	21	0.035073283		
40	21	0.035794221		
41	21	0.035327647		
42	21	0.03501156		
43	21	0.034839785		
44	21	0.035085114		
45	21	0.034288329		
46	24	0.032787719	0.02989137	0.00239568
47	24	0.032139173		
48	24	0.03236147		
49	24	0.032947254		
50	24	0.028859457		
51	24	0.029445851		
52	24	0.027741543		
53	24	0.028028783		
54	24	0.027311966		
55	24	0.027290484		
56	27	0.04866844	0.046021439	0.001493144
57	27	0.048405063		
58	27	0.044544714		
59	27	0.045752979		
60	27	0.04466398		
61	27	0.044244212		
62	27	0.045965955		
63	27	0.045768383		
64	27	0.045952916		
65	27	0.046247749		
66	30	0.029307697	0.026814223	0.001186757
67	30	0.028548822		
68	30	0.029121009		
69	30	0.027857985		
70	30	0.027242585		
71	30	0.026570321		
72	30	0.026159675		
73	30	0.025861586		
74	30	0.02592397		
75	30	0.02577665		

76	33	0.049846079	0.048366968	0.002623562
77	33	0.045668294		
78	33	0.045455227		
79	33	0.044984574		
80	33	0.045906164		
81	33	0.048896116		
82	33	0.052287372		
83	33	0.050199868		
84	33	0.050795235		
85	33	0.049630746		

	Specimen: Corrosion 0 deg.			
Corrosion				
Day 101				
File name	Distance (in.)	Amplitude	Avg.	Standard Deviation
1	6	0.1960715	0.196157725	0.002564117
2	6	0.1907404		
3	6	0.1972028		
4	6	0.191852		
5	6	0.1951337		
6	6	0.1981195		
7	6	0.1976462		
8	6	0.1985838		
9	6	0.193676		
10	6	0.1978735		
11	6	0.1958652		
12	6	0.1944164		
13	6	0.1970883		
14	6	0.1986847		
15	6	0.1994117		
16	9	0.1357545	0.137978838	0.002157072
17	9	0.1341808		
18	9	0.134562		
19	9	0.1387025		
20	9	0.1379727		
21	9	0.1395579		
22	9	0.1398866		

23	9	0.1386685		
24	9	0.1376031		
25	9	0.1377772		
26	9	0.1412159		
27	9	0.139478		
28	9	0.1396959		
29	9	0.1395741		
30	9	0.135053		
31	12	0.0775685	0.078014642	0.000282699
32	12	0.0773325		
33	12	0.0767729		
34	12	0.0776317		
35	12	0.0758959		
36	12	0.0764287		
37	12	0.0764029		
38	12	0.0774498		
39	12	0.0778147		
40	12	0.0782145		
41	15	0.0903029	0.092598831	0.000864077
42	15	0.0909364		
43	15	0.0921628		
44	15	0.0931493		
45	15	0.0930739		
46	15	0.0927578		
47	15	0.0931381		
48	15	0.0928173		
49	15	0.0906191		
50	15	0.0930724		
51	18	0.0498342	0.055313985	0.006459765
52	18	0.0480132		
53	18	0.0475363		
54	18	0.0461473		
55	18	0.0597956		
56	18	0.0602557		
57	18	0.0603471		
58	18	0.060701		
59	18	0.060139		
60	18	0.0603705		
61	21	0.0658739	0.065225503	0.001591611
62	21	0.0664143		
63	21	0.0660269		

64	21	0.066353		
65	21	0.0664806		
66	21	0.0661942		
67	21	0.0655476		
68	21	0.0645169		
69	21	0.0627661		
70	21	0.0620816		
71	24	0.0352114	0.034568296	0.000826294
72	24	0.0347951		
73	24	0.0345181		
74	24	0.034362		
75	24	0.0350244		
76	24	0.0360163		
77	24	0.0330099		
78	24	0.0348256		
79	24	0.0341782		
80	24	0.0337419		
81	27	0.0487786	0.046997464	0.001950529
82	27	0.0491884		
83	27	0.048918		
84	27	0.0486288		
85	27	0.0477309		
86	27	0.0469328		
87	27	0.0461946		
88	27	0.0451097		
89	27	0.0443726		
90	27	0.0441203		
91	30	0.0323908		0.000530523
92	30	0.0316469		
93	30	0.0322888	0.032468459	
94	30	0.0319318		
95	30	0.0331531		
96	30	0.0319528		
97	30	0.0330078		
98	30	0.0330438		
99	30	0.0319274		
100	30	0.0324421		
101	33	0.0414271	0.037633753	0.002312393
102	33	0.0407489		
103	33	0.0397432		
104	33	0.0382699		

105	33	0.0375706		
106	33	0.0360213		
107	33	0.0361518		
108	33	0.0356758		
109	33	0.0357136		
110	33	0.0350153		

	Specimen: Corrosion 0 deg.			
Corrosion				
Day 175				
File name	Distance (in.)	Amplitude	Avg.	Standard Deviation
1	9	0.174652021	0.166533215	0.004874744
2	9	0.162069673		
3	9	0.163658702		
4	9	0.165574207		
5	9	0.166711472		
6	12	0.113106124	0.112145788	0.002371286
7	12	0.108589801		
8	12	0.109129962		
9	12	0.112262656		
10	12	0.111372438		
11	12	0.114824295		
12	12	0.116396281		
13	12	0.112853104		
14	12	0.110889256		
15	12	0.112033964		
16	15	0.093808961	0.099158456	
17	15	0.099231442		
18	15	0.09925552		
19	15	0.10128353		
20	15	0.097268375		
21	15	0.098518733		
22	15	0.101579847		
23	15	0.101549173		
24	15	0.099930517		
25	18	0.080550237	0.075310542	0.003454668
26	18	0.081234552		
27	18	0.075272157		
28	18	0.071423352		

29	18	0.071706553		
30	18	0.074267992		
31	18	0.07455369		
32	18	0.075255213		
33	18	0.073531136		
34	21	0.07720553	0.078308117	0.001781766
35	21	0.077714087		
36	21	0.078521388		
37	21	0.078161469		
38	21	0.077268922		
39	21	0.083070789		
40	21	0.076888023		
41	21	0.078690997		
42	21	0.077304293		
43	21	0.078255672		
44	24	0.065687039	0.065305886	0.001242104
45	24	0.063359168		
46	24	0.064249875		
47	24	0.066735922		
48	24	0.063696171		
49	24	0.064818479		
50	24	0.065477676		
51	24	0.065982023		
52	24	0.067024367		
53	24	0.066028139		
54	27	0.05088282	0.0547752	0.005342643
55	27	0.051130848		
56	27	0.049775247		
57	27	0.044430666		
58	27	0.056001588		
59	27	0.058451475		
60	27	0.05871231		
61	27	0.059155017		
62	27	0.059409214		
63	27	0.059802813		
64	30	0.0405307	0.038166585	0.003580893
65	30	0.035493239		
66	30	0.034856398		
67	30	0.034121261		
68	30	0.035131304		
69	30	0.034659006		

70	30	0.040183603		
71	30	0.041843229		
72	30	0.0424524		
73	30	0.042394711		
74	33	0.047265926	0.047684913	0.000939776
75	33	0.049271339		
76	33	0.048664069		
77	33	0.048064387		
78	33	0.047674139		
79	33	0.045850803		
80	33	0.047872834		
81	33	0.047970326		
82	33	0.047163619		
83	33	0.047051691		

	Specimen: Corrosion 33 deg.			
Corrosion				
Ultragel II				
File name	Distance (in.)	Amplitude	Avg.	Standard Deviation
1	9	0.136009361	0.141178052	0.007875924
2	9	0.133973217		
3	9	0.13480611		
4	9	0.134932665		
5	9	0.134744762		
6	9	0.135198498		
7	9	0.135172878		
8	9	0.13556783		
9	9	0.134701751		
10	9	0.149528903		
11	9	0.149136852		
12	9	0.148896135		
13	9	0.152310975		
14	9	0.151683608		
15	9	0.151007237		
16	12	0.096250092	0.095347378	0.001162308
17	12	0.095550813		
18	12	0.096919853		
19	12	0.094149955		
20	12	0.09507235		

21	12	0.094267489		
22	12	0.096491907		
23	12	0.095200269		
24	12	0.09623313		
25	12	0.093337921		
26	15	0.074725763	0.074675614	0.000598335
27	15	0.074688041		
28	15	0.075483172		
29	15	0.075671486		
30	15	0.07415704		
31	15	0.074486913		
32	15	0.074871704		
33	15	0.074649849		
34	15	0.074428593		
35	15	0.073593579		
36	18	0.043801133	0.065088865	0.007201535
37	18	0.064233128		
38	18	0.066504016		
39	18	0.066432182		
40	18	0.06655954		
41	18	0.066835837		
42	18	0.068642605		
43	18	0.067258192		
44	18	0.068421715		
45	18	0.069637081		
46	18	0.067652083		
47	21	0.035443079	0.035098723	0.000395379
48	21	0.034969048		
49	21	0.035155169		
50	21	0.035073283		
51	21	0.035794221		
52	21	0.035327647		
53	21	0.03501156		
54	21	0.034839785		
55	21	0.035085114		
56	21	0.034288329		
57	24	0.032787719	0.02989137	0.00239568
58	24	0.032139173		
59	24	0.03236147		
60	24	0.032947254		
61	24	0.028859457		

62	24	0.029445851		
63	24	0.027741543		
64	24	0.028028783		
65	24	0.027311966		
66	24	0.027290484		
67	27	0.04866844	0.046021439	0.001493144
68	27	0.048405063		
69	27	0.044544714		
70	27	0.045752979		
71	27	0.04466398		
72	27	0.044244212		
73	27	0.045965955		
74	27	0.045768383		
75	27	0.045952916		
76	27	0.046247749		
77	30	0.029307697	0.02723703	0.001386335
78	30	0.028548822		
79	30	0.029121009		
80	30	0.027857985		
81	30	0.027242585		
82	30	0.026570321		
83	30	0.026159675		
84	30	0.025861586		
85	30	0.02592397		
86	30	0.02577665		
87	33	0.049846079	0.048366968	0.002623562
88	33	0.045668294		
89	33	0.045455227		
90	33	0.044984574		
91	33	0.045906164		
92	33	0.048896116		
93	33	0.052287372		
94	33	0.050199868		
95	33	0.050795235		
96	33	0.049630746		

APPENDIX B: HCP MEASUREMENTS

Specimen: Corrosion 0 deg.		
Corrosion (HCP Data)		
Day 30		
Distance (in.)	mV	Avg.
12	-799	-799
18	-278	-278
24	-320	-320
30	-351	-351

Specimen: Corrosion 0 deg.		
Corrosion (HCP Data)		
Day 101		
Distance (in.)	Amplitude	Avg.
12	-516	-516
18	-513	-513
24	-512	-512
30	-521	-521

Specimen: Corrosion 33 deg.		
Corrosion (HCP Data)		
Day 30		
Distance (in.)	Amplitude	Avg.
12	134	134
18	-190	-190
24	-161	-161
30	-201	-201

Specimen: Corrosion 33 deg.		
Corrosion (HCP Data)		
Day 101		
Distance (in.)	Amplitude	Avg.
12	-479	-479
18	-467	-467
24	-476	-476
30	-510	-510